Hybrid machine learning for digital soil mapping across a longitudinal gradient of contrasting topography, climate and vegetation

Rodrigo de Queiroga Miranda[1,2], Rodolfo L. B. Nóbrega[3], Estevão Lucas Ramos da Silva[4], Jadson Freire da Silva[5], José Coelho de Araújo Filho[4], Magna Soelma Beserra de Moura[5], Alexandre Hugo Cezar Barros[4], Alzira Gabrielle Soares Saraiva Souza[6], Anne Verhoef[7], Wanhong Yang[2], Hui Shao[2], Raghavan Srinivasan[8,9], Feras Ziadat[10], Suzana Maria Gico Lima Montenegro[11], Maria do Socorro B. Araújo[12], and Josiclêda Domiciano Galvíncio[1]

[1]PRODEMA, Universidade Federal de Pernambuco, Recife, Brazil

[2]University of Guelph, Department of Geography, Guelph, Ontario, N1G 2W1, Canada

[3]Imperial College London, Georgina Mace Centre for the Living Planet, Department of Life Sciences, Silwood Park Campus, Buckhurst Road, Ascot, SL5 7PY, UK

[4]Brazilian Agricultural Research Corporation – Embrapa Soils, Recife, Pernambuco, Brazil

[5]Brazilian Agricultural Research Corporation – Embrapa Semi-arid Region, Petrolina, Pernambuco, Brazil

[6]Federal Institute of Education, Science and Technology of Bahia, 45680-000, Uruçuca, Bahia, Brazil

[7]The University of Reading, Department of Geography and Environmental Science, Reading, UK

[8]Spatial Sciences Laboratory, Texas A&M University, College Station, USA

[9]Blackland Research and Extension Center, Agrilife Research, Temple, USA

[10]Food and Agriculture Organization of the United Nations (FAO), 00153 Rome, Italy

[11]Dept. de Engenharia Civil, Universidade Federal de Pernambuco, Recife, Pernambuco, Brazil

[12]Departamento de Ciências Geográficas, Universidade Federal de Pernambuco, Recife, Brazil

Correspondence to: Rodolfo L. B. Nóbrega (r.nobrega@imperial.ac.uk)

Abstract. Environmental models often require soil maps to represent the spatial variability of soil properties. However, mapping soils using conventional in situ survey protocols is time-consuming and costly. As an alternative, Digital Soil Mapping (DSM) offers a fast-mapping approach that has the potential to estimate soil properties and their interrelationships over large areas. In this study, we address the currently outdated spatial information on soil properties across a tropical region (approx. 98,000 km^2) with a ~700-km longitudinal gradient of contrasting topography, climate, and vegetation in Brazil by developing and applying statistical soil models for this region using a novel hybrid machine learning (HML) framework. This framework reduces prediction redundancies due to high multicollinearity by implementing a recursive feature selector algorithm for input selection. The hybrid framework's core is composed of the Soil-Landscape Estimation and Evaluation Program (SLEEP) and a calibrated Gradient Boosting Model (GBM) capable of modeling the spatial distribution of soil properties at multiple soil depths. The use of SLEEP and GBM allowed us to explain the spatial distribution of various basic physical and chemical soil properties and their environmental modulators. The model training and testing approach used six topographical, ten meteorological and two vegetation properties, and data from 223 soil profiles across the study area. Our models demonstrated a consistent performance with spatial extrapolations exhibiting r^2 values ranging from 0.79 to 0.98, and percent bias (PBIAS) from -1.39 to 1.14%. The properties related to topographic and climatic conditions were dominating when estimating the number of soil layers, percentage of silt and the sum of bases. Our framework features high flexibility, while reducing capital investments and increasing accuracy when compared to traditional mapping protocols that require extensive surveys.

Keywords: Gradient Boosting Model, Decision trees, SLEEP, Soil properties, Tropics, Pernambuco.

1 Introduction

Soils are a key component in many landscape models that focus on providing solutions to global environmental issues such as food and water scarcity, unsustainable energy production, and biodiversity losses (Bouma and McBratney, 2013). For a more comprehensive understanding of the role of soils in these global challenges, as well as its interactions with other environmental factors, it is necessary to robustly map the spatial distribution of soil properties. Soil mapping is complex and has been one of the most time demanding and expensive tasks in soil science (Mendonça-Santos and Santos, 2006; Li and Heap, 2014). Most of the existing maps were produced using the conventional soil survey protocol (Hartemink et al., 2012), which remains the most adopted approach to record the highly variable soil properties in landscapes. However, this surveying approach has been criticized for being heuristically dependent on the practical knowledge of pedologists and for deriving interpretations using sometimes insufficient or incomplete datasets (Scull et al., 2003).

Digital Soil Mapping (DSM) is an integrated complementary alternative that has been increasingly gaining adoption as a tool to map soil properties. DSM reduces both survey time and costs (Kempen et al., 2012; McBratney et al., 2003), and it improves the accessibility to soil data with more frequent updates (Lagacherie and McBratney, 2006); it consists of establishing statistical relationships between field information obtained from soil point sampling and environmental data related to soil forming processes, e.g., relief, climate, parent material, and vegetation parameters, to produce models capable of extrapolating data with high resolution (Scull et al., 2003). Numerous studies in Europe (Poggio and Gimona, 2017; Ballabio et al., 2016; Tóth et al., 2017; Adhikari et al., 2014), Africa (Ramifehiarivo et al., 2017; Akpa et al., 2016), North and South America (Padarian et al., 2017; Guevara et al., 2018;

Hartemink et al., 2012), and Oceania (Teng et al., 2018; Gray et al., 2016) used DSM to reduce soil mapping costs over large areas. More specifically, some of them used 3D radar products to acquire high spatial resolution soil information either through data extrapolation using regressors (Adhikari et al., 2014) or disaggregation with machine learning (ML) techniques (Ellili-Bargaoui et al., 2020). Some of these studies contributed to existing regional datasets (Teng et al., 2018) or global datasets such as the GlobalSoilMap project (Ballabio et al., 2016; Rahmati et al., 2018). Others analyzed and discovered new relationships between soil properties and soil-forming processes (Ramifehiarivo et al., 2017). DSM has also been used to find potential hotspots for carbon sequestration and to support sustainable land management strategies, while providing high quality datasets that are widely applicable (Akpa et al., 2016; Guevara et al., 2018; Gray et al., 2016). These data can be coupled with mathematical functions to estimate soils properties for a range of socioeconomical purposes such as water and agricultural management, design of crop rotation scenarios, and urban planning (Padarian et al., 2017).

The methodological core of DSM includes mathematical models capable of performing spatial extrapolations of soil properties at multiple spatial scales (e.g., Barros et al., 2013; Laurent et al., 2017; Saxton and Rawls, 2006; Tomasella et al., 2000; Wang et al., 2018; Zeraatpisheh et al., 2019). These models can predict the distribution of a given soil property horizontally, e.g., over the topsoil of a landscape, or vertically, i.e., along soil profiles. In soil science, spatial extrapolations are usually made by (i) applying a conceptual model to the survey area to simulate the distribution of soil patches (Scull et al., 2003; Silva et al., 2001), (ii) using geostatistical interpolations (Li and Heap, 2014), (iii) delimiting geographical subdivisions where environmental processes follow a relatively homogeneous pattern, such as the facets described by Ziadat et al. (2015), or (iv) by applying pedotransfer functions (PTFs) to properties of each soil location. PTFs are predictive mathematical equations that aim to use basic soil information to derive other soil properties that are often costly to measure, such as the water retention curve, or related parameters, e.g., field capacity and wilting point (Hugo et al., 2014). When combining both above-mentioned types of predictive tools to perform 3D extrapolations, high uncertainties are expected, especially for the vertical extrapolations because information is required across the soil profile that is rarely available (Yost and Hartemink, 2020).

In Brazil, many polynomial PTFs have been calibrated at both national (Tomasella et al., 2000) and sub-national scales (Barros et al., 2013; Oliveira et al., 2006, 2002). However, for many soil properties or geographic regions, certain PTFs might not provide sufficiently accurate parameter estimates due to their excessive number of polynomial terms that lead to overfitting (Hawkins, 2004). For example, mathematical regressions calibrated for temperate climate zones and applied to the tropics often do not return realistic soil parameters, e.g., Tomasella and Hodnett (1998). These applications may lead to improper soil use and management recommendations. To avoid misapplications that produce inconsistent soil maps, it is important to develop robust geostatistical relationships between predictive models and regional characteristics in Brazil (Hugo et al., 2014; Vieira, 2000).

Compared to popular linear regression models, Machine Learning (ML) techniques have been increasingly applied to fit the relationships between soil properties and environmental parameters. These techniques include a set of models capable of detecting non-linear patterns, such as generalized linear models (Beguería et al., 2013), random forest (Esfandiarpour-Boroujeni et al., 2020; Pahlavan-Rad et al., 2020; Poppiel et al., 2021), cubist (Taghizadeh-mehrjardi et al., 2016), and support vector machine (Esfandiarpour-Boroujeni et al., 2020). These models have been successfully applied to generate a wide variety of data types, which is compelling because soil properties often do not follow a normal distribution, but an exponential, Poisson, Bernoulli or uniform distribution instead (Hitziger and Ließ, 2014). If trained properly, ML techniques allow for accurate predictions, whereas other approaches with underlying assumption on distributions may not be applicable or even fail to produce any values (Taghizadeh-mehrjardi et al., 2016), e.g., a regression may require the calculation of the square root or logarithm of negatives values. In fact, Behrens et al. (2018) suggest that ML techniques might even eliminate the need for further steps to correct biases during the mapping process because they commonly only produce residuals that do not exhibit any spatial dependence.

The use of ML in DSM can provide soil products for improving modeling performance in other scientific fields, since soil maps are used as spatially distributed inputs for other widely used models, such as land surface models, e.g., CABLE (Wang et al., 2011), JULES (Clark et al., 2011; Best et al., 2011) and ORCHIDEE (Krinner et al., 2005), and some widely applied hydrological models, e.g., Soil and Water Assessment Tool (SWAT; Arnold et al., 1998), and Soil and Water Integrated Model (SWIM; Krysanova et al., 1998). Bossa et al. (2012) evaluated the impact of different soil mapping concepts in hydrological models and demonstrated that it strongly influences modeling outputs. In this context, the mapping approach and the soil database scale are important and directly affect many modeling steps (Bossa et al., 2012). Thus, environmental modeling and other soil data applications need adequate spatial characterization of soil properties (Ziadat et al., 2015; Montzka et al., 2017).

Currently, soil maps for the tropics often shows a coarse spatial soil property aggregation, which generalizes soil variability into average values. This occurs because the common statistical techniques applied to perform extrapolations are heavily dependent on how dense the collection of soil profiles is;

and this is generally sparse due to financial and temporal limitations. In this study, we addressed the growing need for soil models that produce improved information about the spatial variability of soil properties in the tropics, by developing and applying a novel hybrid machine learning (HML) framework to a region with a ~700-km longitudinal gradient of contrasting topography, climate, and vegetation in a tropical region. Our goal was to develop and evaluate a hybrid framework that integrates Gradient Boosting Models (GBM) with a soil landscape attribute model that allowed for (1) predicting and comparison of spatial distributions of basic soil properties (physical and chemical properties), and (2) for a better interpretation of major environmental modulators of the soil spatial distribution in this region.

2 Methodology

2.1 Methodology overview

In this study we develop and apply a novel HML framework integrating the Soil-Landscape Estimation and Evaluation Program (SLEEP) and a calibrated Gradient Boosting Model (GBM). HML can be understood as a seamlessly combination of algorithms from different areas of knowledge to complement each other for higher predictive power than a standalone ML algorithm, e.g., Artificial Neural Network and Vector Support Machine. By integrating SLEEP and GBM, we created a promising framework capable of predicting soil data over large areas. Our methodology for applying the framework comprises a three-step process that starts with the collection and preprocessing of six topographical, ten meteorological, and two vegetation properties acquired from different data sources ranging from remotely sensed datasets to meteorological stations. These are the independent variables to be correlated with *in* *situ* soil granulometry and carbon content to make subsequent horizontal and vertical predictions of these basic soil properties. We used the Soil-Landscape Estimation and Evaluation Program (SLEEP; Ziadat et al., 2015) to create a non-distributed grid formed by facets, which, in this study, are treated as the smallest area that reflect a single homogenous unit where soil formation factors might produce homogeneous types of soils. To create these facets, we first delineated watersheds in our study area. Each watershed was divided into multiple catchments, and then the facets were defined by the division of the catchments into two parts, i.e., each side of their main drainage stream (Ziadat et al., 2015). The size of the catchments is determined by a user-defined threshold assigned during stream definition. The smaller this threshold, the denser is the stream network, resulting in a greater number of delineated catchments and facets. Once the facets were created, we aggregated them based on their slope similarity, which ultimately creates contiguous patches. The patches allowed us to reduce the number of facets by grouping them in a single mapping unit. These are especially useful to reduce the processing time when working with large areas, and to avoid the 'salt-and-pepper' noise in the mapping process. Then, we simulated the basic soil properties in each patch at multiple depths by calibrating one model for each soil basic property using ML instead of simple multiple regressions because they can capture a wider range of data distributions. The calibration mechanism is composed of a recursive feature selector and a randomized searcher, which were configured to perform a 2-fold cross-validation. At the end of this step, all patches are turned into virtual soil profiles, namely simulated soil patches with their own depth-dependent simulated physical and chemical properties. The uncertainty was calculated for each property to characterize the error consistency for each simulated value. Finally, in the third step, the entire dataset composed of virtual profiles was complemented with further simulated soil parameters obtained with a range of PTFs, and an analysis of the relationship between our estimates and the land-use of the study area. The entire modeling algorithm developed and applied in this study is open source, written in Python versions 2.7.15 and 3.6.9 and available at https://github.com/razeayres/sleepy.

2.2 Study area

The study area is in the Northeast Brazil; it covers an area of approx. 98,000 km^2, and closely follows the domain of the state of Pernambuco (Fig. 1). This region exhibits a longitudinal gradient of contrasting topography, climate and vegetation. The elevation ranges from approx. 0 to over 1,150 m a.s.l. in a variable gradient from East to West. This region is influenced by three meteorological phenomena, namely Frontal Systems (FS), Upper Tropospheric Cyclonic Vortices (UTCV), and the Inter Tropical Convergence Zone (ITC) (Salgueiro et al., 2016). There are three predominant climate types (Köppen's classification) in the study are: hot semi-arid (steppe) climate (BSh; 61.4% of the area), tropical with dry summer (As; 32.7%) and tropical monsoon (Am; 4.9%); the remaining 1% is composed of areas with a tropical climate with dry winter (Aw; 0.1%), humid subtropical with dry winter and hot (Cwa; 0.3%) and temperate summer (Cwb; 0.3%), and with dry and hot summer (Csa; 0.3%) (Alvares et al., 2013). Precipitation has a high spatial variability (Souza et al., 2021) with the annual mean precipitation rates reaching approx. 2,000 mm in the East, and decreasing westwards to less than 400 mm. As for the vegetation, near the coast, the predominant land-uses are Atlantic rain forest and rainfed croplands, which are composed of a mosaic of sugarcane plantations and fruticulture (Project MapBiomas - Collection 5 of Brazilian Land Cover & Use Map Series). With the climate becoming drier, the vegetation changes to a seasonally dry tropical forest, i.e., the Brazilian Caatinga. Pastures become a common land-use activity, and the soil gets shallower and rocky (Souza et al., 2021). In the middle transition, some high-altitude areas create microclimatic conditions that favor rainfed crops of corn and beans, and mixed natural vegetation formations. According to the Brazilian system of soil classification (and FAO system of soil classification), the dominant soils are, respectively, *Argissolos* (i.e., Acrisols and Lixisols) (25% of the area), *Neossolos* (i.e., Leptosols, Arenosols, Regosols, or Fluvisols) (32%) and *Planossolos* (i.e., Planosols and Solonetz) (16%), *Latossolos* (i.e., Ferralsols) (9%) and *Luvisolos* (i.e., Luvisols) (9%) (Silva et al., 2001; Filho et al., 2014). The geology maps for the state of Pernambuco show predominantly (90%) pre-Cambrian rocks belonging to the São Francisco Craton and the Borborema Province, and the remaining area is mainly composed by Paleomesozoic sedimentary basins and Mesocenezoic coastal basins (Torres, 2014).

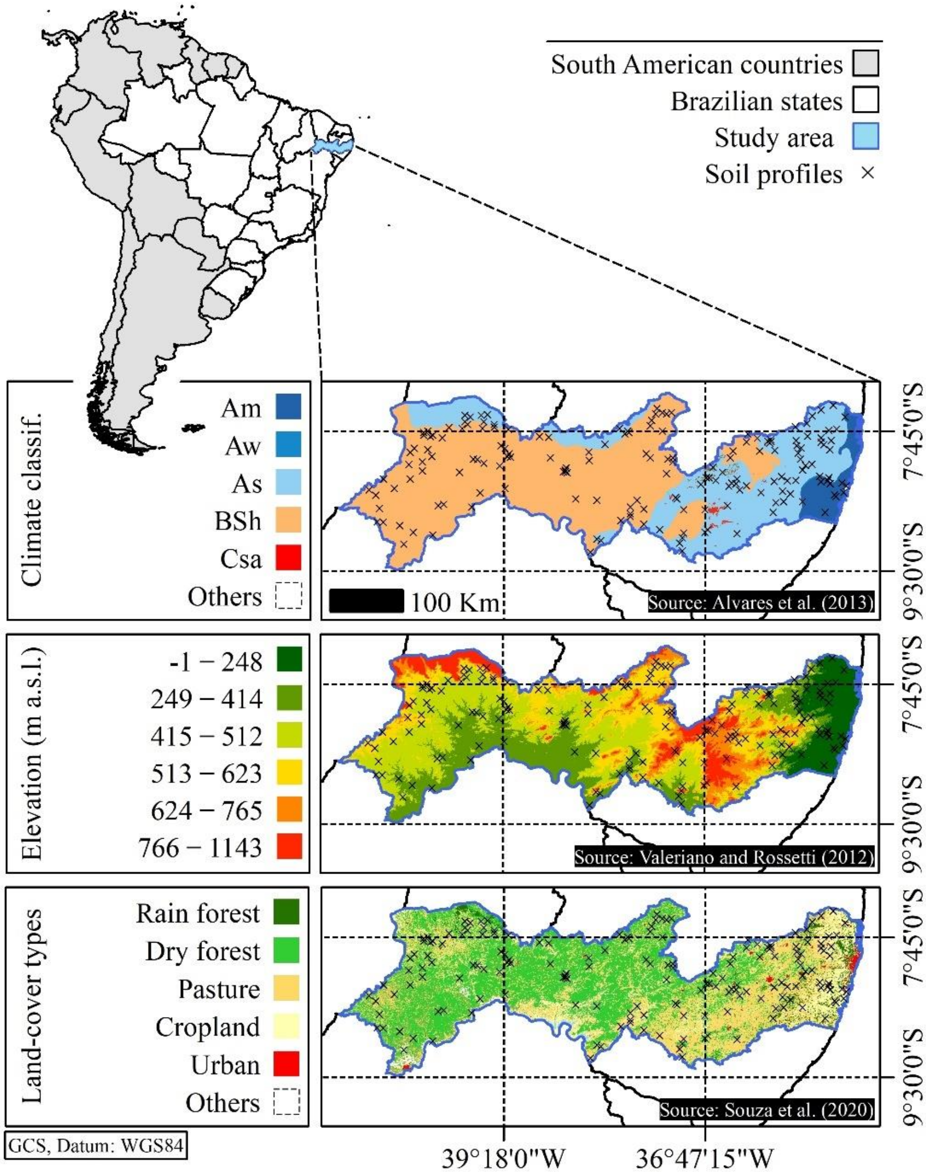

Figure 1: Spatial distribution of the surveyed soil profiles across a longitudinal gradient of environmental conditions over the study area.

2.3 Input data collection

Elevation data: we collected data from the TOPODATA database (http://www.dsr.inpe.br/topodata), which is a bias-corrected version of the data produced by the NASA SRTM (Shuttle radar topography mission) for the Brazilian territory made by the National Institute of Spatial Research (INPE). The data were spatially refined from 3 (approx. 90 m) to 1 arc-second (approx. 30 m) using adjusted kriging models, and it was tested on 40 Brazilian areas with distinct geological settings (Valeriano and Rossetti, 2012). **Soil data:** the georeferenced data regarding morphological (profile depth and number of horizons), physical (particle size distribution) and chemical (Ca^{2+}, Mg^{2+}, K^{+}, Na^{+} and C) properties of the soil were acquired from the Agroecological Zoning of the state of Pernambuco (ZAPE) project of the Brazilian Agricultural Research Corporation (EMBRAPA) (Silva et al., 2001). The ZAPE project focused on the production and organization of a georeferenced database with information on soils, climate, and vegetation that can be used in multiple applications, including sustainable land-use management and agricultural purposes (Silva et al., 2001). The soil database comprises 223 soil profiles distributed over the study area (Fig. 1). **Auxiliary meteorological data:** data for air temperature (°C), air relative humidity (%), solar radiation (MJ m^{-2} day^{-1}), wind speed (m s^{-1}), and precipitation (mm) from the 1961–2016 period were obtained through two open-access databases: daily precipitation data from the Water and Climate Agency of Pernambuco (APAC; http://www.apac.pe.gov.br/meteorologia/monitoramento-pluvio.php), and the other meteorological parameters from the National Water Agency of Brazil (ANA; http://www.snirh.gov.br/hidroweb/publico/medicoes_historicas_abas.jsf). **Auxiliary remote sensed data:** data regarding NDVI (Normalized Difference Vegetation Index) (MOD13A3; composition:

monthly, spatial resolution: 1 km), and LST (Land Surface Temperature) (MOD11A2; composition: 8-days, spatial resolution: 1 km) were downloaded from https://earthdata.nasa.gov/.

Table 1. Summary of variables and parameters with their corresponding descriptions and units.

Variable	Type	Description	Unit
AAT	T	Prefix used to denote accumulated variables	-
ASPECT	T	Downslope direction at each cell	°
CTI	T	Compound Topographic Index	-
CURV	T	Curvature of the surface at each cell	-
DEM	T	Digital elevation model	m
PCTSLP	T	Slope of the surface at each cell	%
LST	V	Land surface temperature	K
NDVI	V	Normalized difference vegetation index	-
DEWPT	C	Mean air relative humidity	fraction (0–1)
PCPMM	C	Mean total monthly precipitation	mm
PCPSKW	C	Skew coefficient for daily precipitation in month	mm
PCPSTD	C	Standard deviation for daily precipitation in month	mm
SOLARAV	C	Mean daily solar radiation for month	MJ m^{-2} day^{-1}
TMPMN	C	Mean daily minimum air temperature	°C
TMPMX	C	Mean daily maximum air temperature	°C
TMPSTDMN	C	Standard deviation for daily minimum air temperature	°C
TMPSTDMX	C	Standard deviation for daily maximum air temperature	°C
WNDAV	C	Mean daily wind speed in month	m s^{-1}
CS	B	Coarse sand content	%
FS	B	Fine sand content	%
L_MAX	B	Number of soil layers	-
SB	B	Sum of Base (Ca^{2+}, Mg^{2+}, K^+ and Na^+)	$cmol_c$ kg^{-1}

SN1	B	Non-sand content	fraction
SOL_BD	B	Moist bulk soil density	g cm^{-3}
SOL_CBN	B	Organic carbon content	%
SOL_CLAY	B	Clay content	%
SOL_ROCK	B	Rock fragments content	%
SOL_SAND	B	Sand content	%
SOL_SILT	B	Silt content	%
SOL_Z	B	Depth from soil surface to bottom of the soil layer	mm
R_v	P	Volume fraction of gravel	cm^3 cm^{-3}
R_w	P	Weight fraction of gravel	g g^{-1}
θ_{1500}	P	Water content at -1500 kPa	m^3 m^{-3}
θ_{33}	P	Water content at -33 kPa	m^3 m^{-3}
θ_S	P	Saturated water content	m^3 m^{-3}
θ_r	P	Residual water content	m^3 m^{-3}
ρ_N	P	Normal density	g cm^{-3}
ρ_R	P	Gravel density	g cm^{-3}
OM	P	Organic matter	%
SOL_AWC	P	Available water capacity of the soil layer	mm mm^{-1}
SOL_K	P	Saturated hydraulic conductivity	mm hr^{-1}
USLE_K	P	USLE equation soil erodibility (K) factor	-
Ψ	P	Matric potential	kPa
α, n and m	P	Shape-fitting parameters of (van Genuchten, 1980)	-

In the second column: T = topography, V = vegetation, C = climate, B = basic property, and P = pedotransfer function parameter.

2.4 Soil survey data description

Our soil dataset consists of the total number of soil horizons (L_MAX), but for the modelling purposes in this study we will be referencing it as the number of soil layers as we did not validate model efficacy on distinguishing horizons with further field experiments. The database also has each soil layer depth from the land surface (SOL_Z; mm), soil clay content (< 0.002 mm; SOL_CLAY; %), silt (> 0.002 and < 0.05 mm; SOL_SILT; %), sand (> 0.05 and < 2 mm; SOL_SAND; %), rock (> 2 mm; SOL_ROCK; %), organic carbon (SOL_CBN; %) and sum of bases (sum of Ca^{2+}, Mg^{2+}, K^{+} and Na^{+}; SB; $cmol_c\ kg^{-1}$). In this study, we define the rock parameter as the sum of the fractions of gravel (> 2 mm and < 2 cm), cobbles (> 2 cm and < 20 cm), boulders (> 20 cm and < 100 cm) and rocks (> 100 cm). The sand fraction was divided into coarse (> 0.2 and < 2 mm; CS) and fine (> 0.05 and < 0.2 mm; FS) (Table 1). All particle classification followed the Brazilian technical standards described in ABNT (1995), and physical and chemical analysis were performed as described in EMBRAPA (1997).

Soil profiles exhibit an average total depth of 1,228 ± 613 mm, ranging from 120 to 2,550 mm. The number of soil layers varies from one to seven and correlates well ($r^2 = 0.89$, p-value < 0.01) with the profile depth (SOL_Z). Rocks exhibit 4.4 ± 11% of total content, and when they are not considered by the soil texture is composed by sand (55 ± 19%), clay (27 ± 14%), and silt (18 ± 9%) (Fig. 2). The low silt content is typical of tropical environments, and it is a common property in the Northeast region of Brazil (Barros et al., 2013; Ottoni et al., 2018), where most sandy soils originate from the quaternary era, and the clayey ones from tertiary and early cretaceous eras (Araújo Filho et al., 2000). These textural patterns determine differences in hydraulic properties between soils in tropical and temperate regions

(Ottoni et al., 2018). For this reason, PTFs developed for temperate climates often provide inaccurate or unrealistic estimates when applied to the tropics (Barros et al., 2013; Tomasella et al., 2000). Organic carbon contents are higher (0.54 ± 0.49%) than the values found by Barros et al. (2013) for the Northeast region of Brazil (0.35%), and lower than the ones for the entire Brazilian territory (0.91 ± 0.78%) (Tomasella et al., 2000).

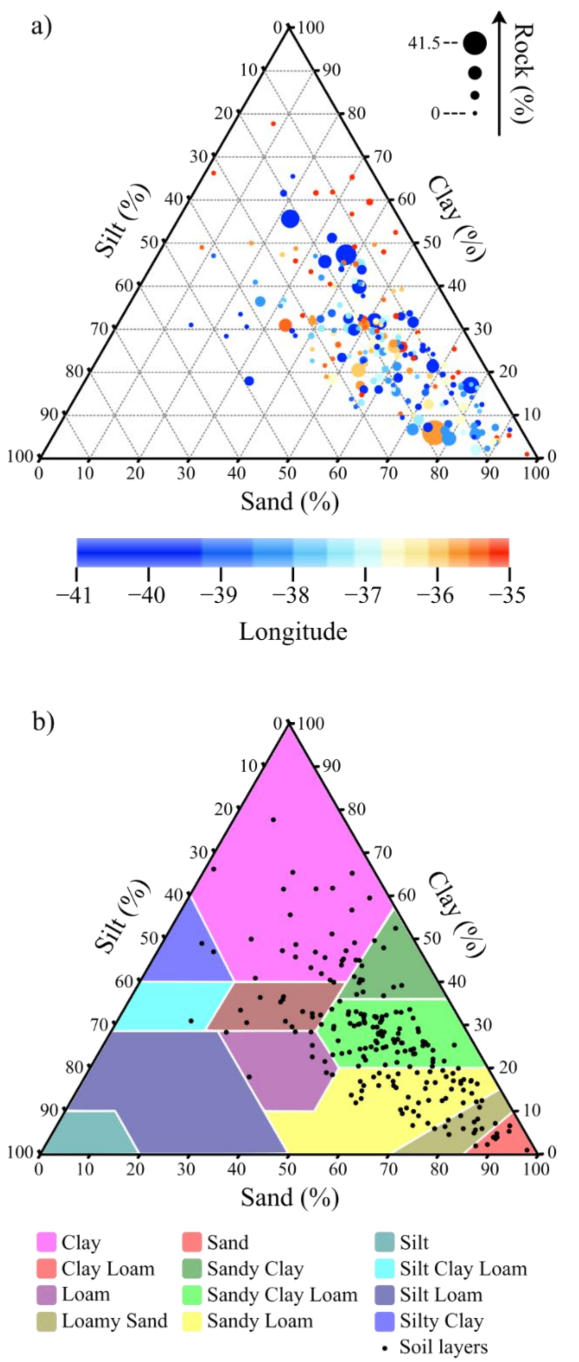

Figure 2: Soil textural distribution for sand, silt and clay upscaled to 100% after removing the fraction of rocks, which is exhibited separately in (a).

2.5 Input preprocessing workflow

As a first step, the data for each soil layer from each soil profile (total of 925 soil layers) were converted into a shapefile. We estimated the organic matter (OM) by multiplying SOL_CBN by 2, as recommended by Pribyl (2010). For all meteorological parameters (Table 1), we calculated means and standard deviations for all months in the data series (multiple months) and considered the maximum and minimum air temperatures as distinct parameters; then the monthly statistics were summed (in case of precipitation) or averaged resulting in 12 historical values. In addition to these statistics, we calculated the skewness of rainfall data distribution following the same logic of temporal aggregation (PCPSKW) using the following equation:

$$\text{PCPSKW} = \frac{d_W \times \sum_{d=1}^{d_W} \left(P_d - \bar{P}\right)^3}{(N-1) \times (N-2) \times \sigma^3} \quad (1)$$

Here d_W is the count of wet days in a month, N is the number of daily data records for a month, P_d is the precipitation on a given day in mm, $\bar{P}$ is the monthly average precipitation, and σ is its standard deviation. For all calculations we only considered years without gaps in the data series for each meteorological station individually, and from these data we derived ten parameters that were used in a spatial interpolation. This interpolation was conducted using the inverse distance weighting (IDW) method at a fixed cell resolution of 0.05°. This method was chosen due to its representativeness in variable terrain area and wide adoption for climate data interpolation, e.g., Tan et al. (2021). Additionally, we performed a leave-one out cross-validation and extracted details on the accuracy of these interpolations (Table 2). As for the remotely sensed data, mosaics and reprojections were created using the MODIS Reprojection

Tool, and scaling and processing of the historical annual images were conducted using the GDAL library (https://gdal.org/). The scaling factors for each product were acquired from the relevant user guides available at https://lpdaac.usgs.gov/.

Table 2. Leave-one-out cross-validation leave-one out of all interpolated meteorological input parameters. The description of the variables can be found in Table 1.

Parameters	Power	Samples	r^2	RMSE	PBIAS
PCPMM (mm)	1.64	6140	0.94	21.34	-0.10
PCPSTD (mm)	1.65	6140	0.83	2.62	-0.17
PCPSKW (mm)	1	6140	0.87	1.33	0.03
TMPMX (°C)	1.63	254	0.94	1.51	0.19
TMPMN (°C)	1.77	254	0.95	1.43	0.88
TMPSTDMX (°C)	2.32	254	0.97	0.24	-0.51
TMPSTDMN (°C)	1	254	0.95	0.30	-0.18
SOLARAV (MJ m^{-2} day^{-1})	1.46	254	0.94	1.00	-0.24
DEWPT (0–1)	1.66	254	0.92	0.04	0.38
WNDAV (m s^{-1})	1.82	254	0.89	1.25	-0.0001

2.6 Spatial modeling

The core of the HML framework combines the Soil-Landscape Estimation and Evaluation Program (SLEEP) and a calibrated Gradient Boosting Model (GBM). Soil data were modeled using the SLEEP model by creating facets, for which basic soil properties, i.e., L_MAX, SOL_Z, SOL_CLAY, SOL_SILT, SOL_SAND, CS, FS, SOL_ROCK, SOL_CBN, and OM, were calculated. The SLEEP model requires three different types of inputs: (i) a digital elevation model (DEM), (ii) a shapefile containing the data observed for each soil profile, and (iii) the auxiliary data including meteorological and vegetation data in raster format (Fig. 3) (Ziadat et al., 2015). In this algorithm, we extract the drainage network following

(Tarboton et al., 1991) by using the size of the catchments to represent 0.001% of the total study area, i.e., on average 1,803 pixels per catchment, which was obtained based on a visual evaluation of different thresholds with a focus on providing high resolution data and satisfactory model processing time. We aggregated the facets based on their slope similarity using the clustering technique Iso Cluster (Richards, 2013) to create patches. Finally, we modified the way the basic properties are modeled, changing it from simple multiple linear regressors to GBMs (Fig. 4). GBM is an ensemble learner that consists of a set of decision trees composed by weak-prediction models (WPM) often prone to overfitting, and, when combined, produces highly accurate outputs. Each of these trees is a rule-based system, where their terminal nodes can either be a WPM, i.e., leaf, or an if-then-else rule over a given input variable, i.e., regular node. The whole trees are created using an iterative sequence of improvements of WPMs (i.e., boosting), while optimizing themselves by reducing a loss function, i.e., gradient (Natekin and Knoll, 2013).

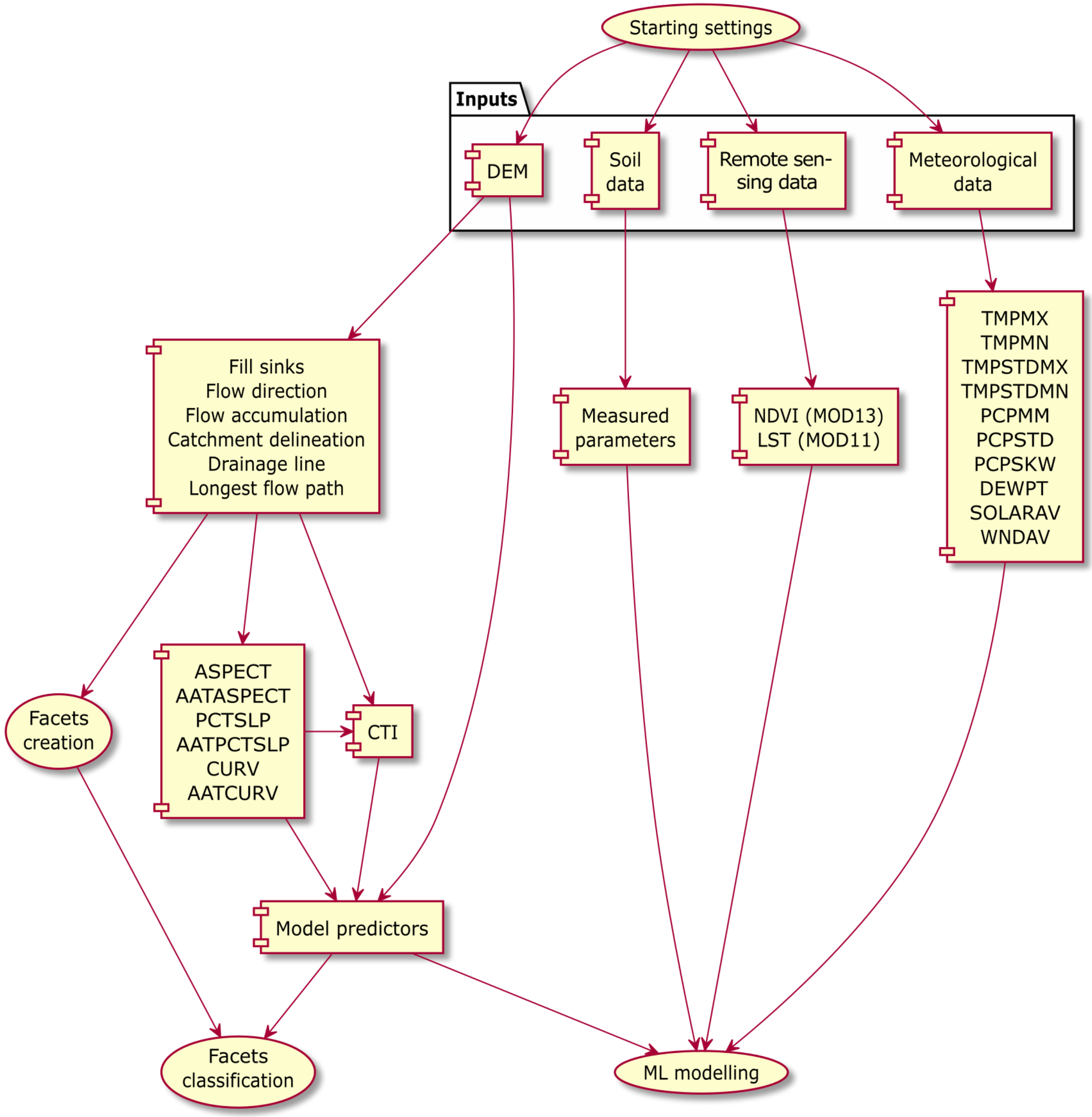

Figure 3: Processing scheme of the adaptation of the SLEEP algorithm (Ziadat et al., 2015). The description of the parameters can be found in Table 1.

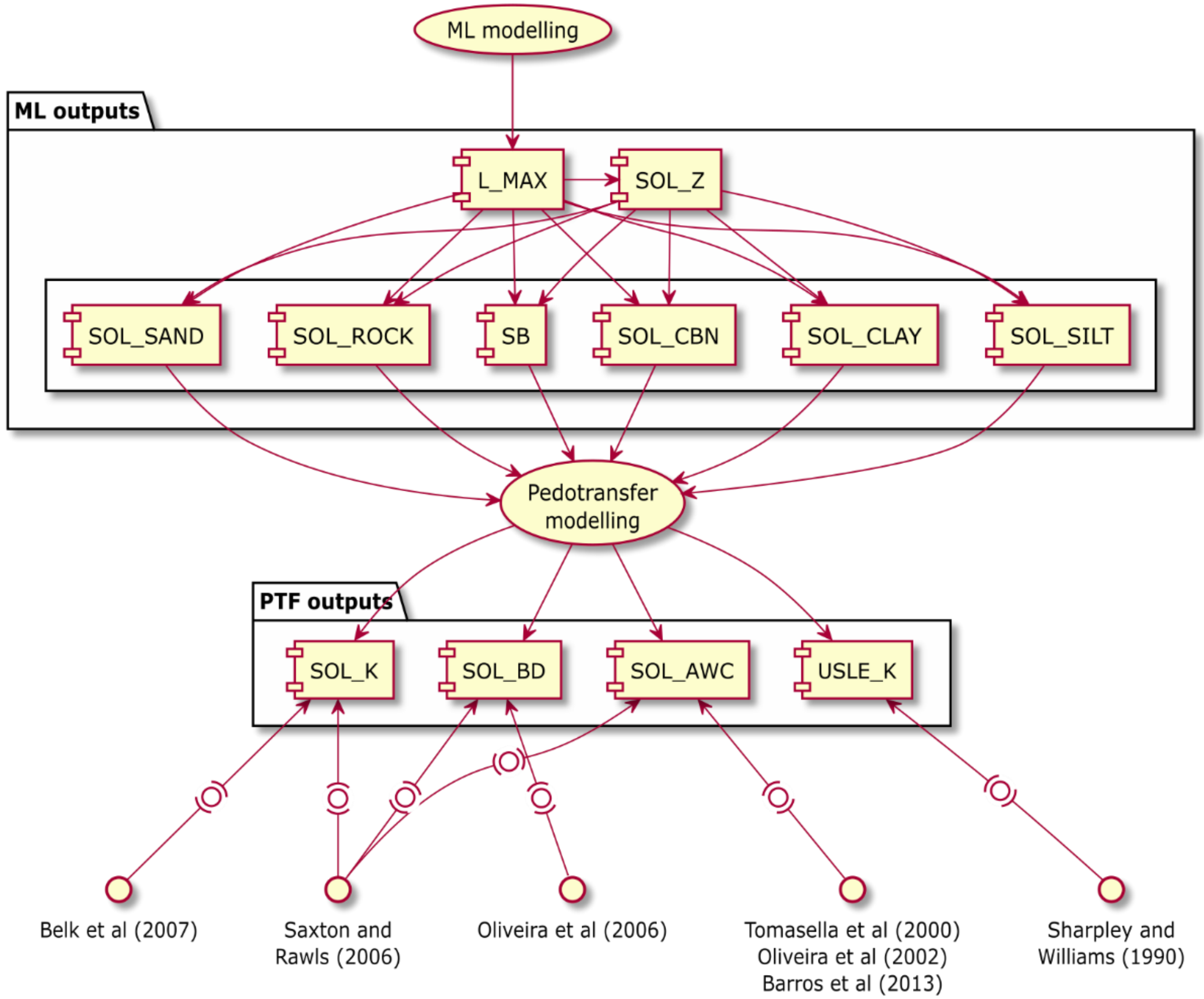

Figure 4: Processing workflow of all model outputs. The top half of this figure explains the machine learning processing of the basic soil characteristics, whereas the bottom half summarizes the PTF-derived products. The description of the parameters can be found in Table 1.

For the GBM processing, two datasets were produced: (i) one composed of only the information from the patches that overlay the observed data for each profile (dataset for fitting), and (ii) consisting of all available input information for every patch in the study area (dataset for prediction). The dataset for fitting was split using the Holdout method at 20%, e.g., Whitney (1971), creating two sub-datasets, where 80% of the records were used for model calibration (training dataset), and the remaining for further model verification (verification dataset) (Fig. 5). The sampling technique used in this process is a variation of the k-fold cross-validation (Wong, 2015), which returns stratified folds containing approximately the same percentage of samples of each target class. When dependent variables were continuous, without classes, a quantile-based discretization function (QCUT) was applied to discretize these variables into equal-sized groups based on sample quantiles, allowing for sampling the entire data distribution. The GBMs had four basic parameters derived from the DEM (Table 1) as input features, namely the downslope direction (ASPECT), the Compound Topographic Index (CTI), the curvature of the surface (CURV) and the slope of the surface (PCTSLP). The CTI is represented by a steady state wetness index as a function of the slope and the upstream contributing area (Moore et al., 1993), and 12 auxiliary data series from remote sensing products and meteorological stations. As targets, they had eight basic soil properties. All inputs and targets are described in Table 1. GBM was used as a multiclass classifier to simulate the number of soil layers, L_MAX; and as regressors for the other targets. SOL_ROCK was estimated as a residual of all textural parameters. Coarse sand (CS) and fine sand (FS) were resampled to total 100%.

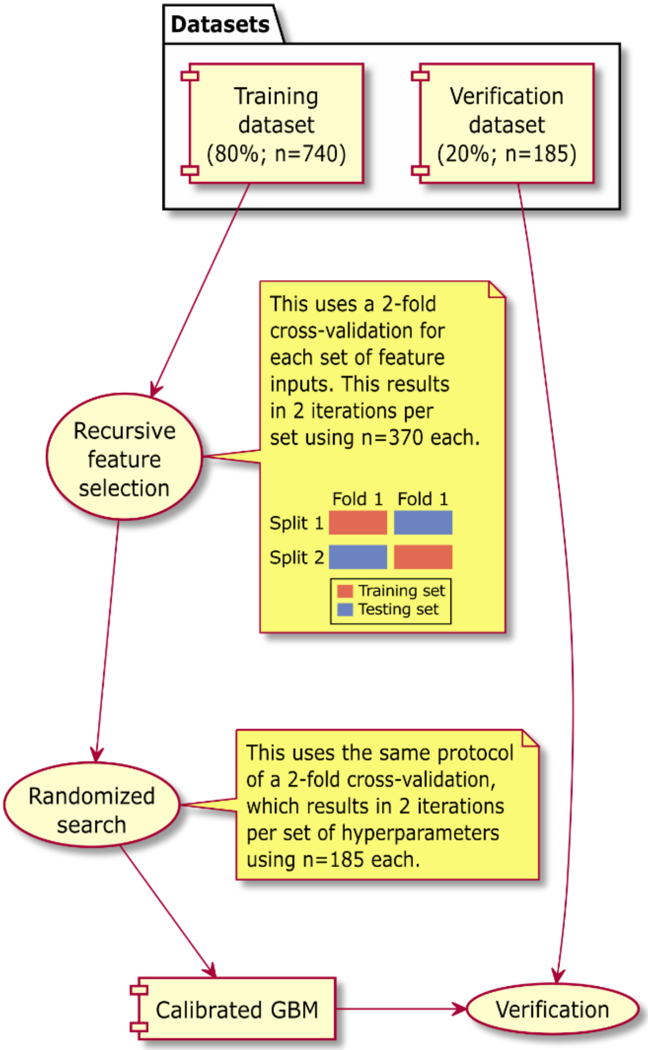

Figure 5: Machine learning processing design for modeling the basic soil properties.

GBMs are often parameterized with only a few control inputs called hyperparameters. They hold the potential to define the final structure of the model and its predictive strength. These hyperparameters must be calibrated; for that purpose, we submitted all our GBMs to a recursive feature selector (RFS; Guyon et al., 2002) configured to perform cross-validation using the k-fold cross-validation at 2-folds, and then a randomized 2-fold calibration to search for the best combination of hyperparameters. The RFS here is an input feature selection algorithm that fits a model and eliminates the weakest ranked inputs recursively, considering each iteration a smaller set of features until the best combination found. The performance indices used in all calibrations were the accuracy (Eq. 2) for the classifiers, i.e., L_MAX, and the coefficient of determination (r^2) (Eq. 3) for the regressors. Further in the analysis, for model verification, the most efficient models were compared to the testing dataset, and the same performance indices plus the Root Mean Square Error (RMSE) (Eq. 4) and Percent Bias (PBIAS) (Eq. 5) were applied. This final verification allowed us to evaluate the potential of the best models to perform extrapolations.

$$\mathbf{Accuracy} = \frac{(\boldsymbol{TP}+\boldsymbol{TN})}{(\boldsymbol{TP}+\boldsymbol{FP}+\boldsymbol{FN}+\boldsymbol{TN})} \quad (2)$$

$$\mathrm{r}^2 = \frac{\sum(obs-\overline{obs})\times(sim-\overline{sim})}{\sqrt{\sum(obs-\overline{obs})^2}\times\sqrt{\sum(sim-\overline{sim})^2}} \qquad (3)$$

$$\mathrm{RMSE} = \sqrt{\frac{\sum(obs-sim)^2}{n}} \qquad (4)$$

$$\mathrm{PBIAS} = \frac{\sum(obs-sim)}{\sum(obs)} \times 100 \qquad (5)$$

TP, FP, FN and TN are the number of True Positives, False Positives, False Negatives and True Negatives, respectively, in a contingency table; obs is the observed value of a given soil layer, and sim is the simulated one, and $\overline{obs}$ and $\overline{sim}$ are average values. Accuracy is a metric of evaluation for classification problems that works well only if the data distribution is not skewed. We then applied the Synthetic Minority Oversampling Technique (SMOTE) to our dataset to solve all possible imbalances by producing a new dataset that has a uniform distribution. This technique forces a balanced learning and an overall better class detection. It introduces biases towards the minority classes by adding more samples to the model learning process from these classes. Details of this technique can be found in Chawla et al. (2002). To calibrate the hyperparameters, we created a set of possible values for each parameter. For n_estimators (NE; number of trees in the forest), it was composed of 100 values varying from 10 to 5,000; for max_depth (MD; maximum number of levels in each decision tree) it was 100 values in the 1–100 interval; and min_samples_leaf (MSL; minimum number of data for a node to persist) and min_samples_split (MSS; minimum number of data placed in a node required to perform a split) were both set to 49 values, varying between 2–50. These four hyperparameters control the potential for overfitting. If n_estimators is excessively high, then the GBM exhibits a robust performance during calibration but has a poor predictive strength during extrapolations. Also, n_estimators must be determined for each individual application, and directly affects the learning rate and processing time. Small values for max_depth are desirable to avoid models learning very localized relations that cannot be accurately extrapolated. The same applies to min_samples_leaf to solve imbalances in samples distribution successfully. The value of min_samples_split has a similar effect as max_depth on the model performance, but here higher values are best to avoid relations highly specific to samples selected for a given tree. These effects are well described in Dormann et al. (2007), Elith et al. (2008) and Hitziger and Ließ (2014). The entire hyperparameter tuning was set to run 4,000 simulations. The calibrated models were applied to predict the basic properties for each patch, creating 64,415 virtual soil profiles. The entire predicted dataset was converted to raster format, and each raster is a different soil attribute.

2.7 Sensitivity and uncertainty analysis

The model sensitivity to input data was calculated as the importance, i.e., a weighted factor of each selected property for the most accurate GBMs. The importance (w) ranges from 0 to 1, where 1 reflects the highest weight a given input can receive in a model, and 0 the lowest. The sum of all weights is 1 for each model. More specifically, w values reflect indirectly how much the performance metric changes every time a given input is used to split a node in the whole model (Natekin and Knoll, 2013).

For the uncertainty analysis of the modeled variables, the selected inputs for each model and patch used in the predictions were classified into two categories (e), i.e., whether they extrapolated the calibration range of values (1) or not (0), as summarized in the following equation:

$$u_f = \sum_{i=0}(e_i \times w_i), \quad (6)$$

where u_f is the uncertainty of each model; patch, e_i, is the binary category that reflects the extrapolation and w_i is its importance in the model (weight) of a given selected input i. As u_f gets close to 1, extrapolation is greater and so is its associated uncertainty. The contrary happens when it approaches 0, which means that all inputs used for a given prediction were in the range of values used for calibration.

2.8 Application of pedotransfer functions

All data from the virtual soil profiles were submitted to a series of pre-established PTFs to estimate four soil properties: SOL_BD (moist bulk density; g cm^{-3}), SOL_AWC (available water capacity; mm mm^{-1}), SOL_K (saturated hydraulic conductivity; mm hr^{-1}), and USLE_K (factor K from the USLE equation; unitless). SOL_K and USLE_K were modeled using the equations described in Saxton and Rawls (2006) and Belk et al. (2007), and Sharpley and Williams (1990), respectively (Table 3). The calculation of

SOL_AWC created a factorial design in our analysis. It was acquired with the equations from Saxton and Rawls (2006), Tomasella et al. (2000), Oliveira et al. (2002) and Barros et al. (2013) (Table 4). Saxton and Rawls (2006) produced PTFs using a soil dataset from an exhaustive soil sampling across the entire United States. Tomasella et al. (2000) used a similar database for Brazil, while Barros et al. (2013) used data for the Northeast region of Brazil only. Finally, Oliveira et al. (2002) created PTFs with data that originated strictly from the state of Pernambuco. All SOL_AWC models require SOL_BD as an input. Thus, SOL_BD from Saxton and Rawls (2006) was coupled with their own SOL_AWC model, while SOL_BD from Oliveira et al. (2006) was used in the models of Tomasella et al. (2000), Oliveira et al. (2002) and Barros et al. (2013). This resulted in 32 different complete sets of PTFs that can be used to estimate the five soil properties.

Table 3. Pedotransfer models for soil conductivity (SOL_K) Saxton and Rawls, 2006; Belk et al., 2007) and K-factor from USLE equation (USLE_K) (Sharpley and Williams, 1990). Please check Table 1 for the meaning of the acronyms.

Models	Eq.
• $\text{SOL\_K} = 1930 \times (\theta_S - \theta_{33})^{(3-\lambda)}$	(7)
• $\lambda = \frac{1}{B}$	
○ $B = [\ln(1500) - \ln(33)]/[\ln(\theta_{33}) - \ln(\theta_{1500})]$	
• $\text{SOL\_K} = \left\{\left[58 \times \left({SOL\_Z}/{1000}\right)^{-0.9}\right] \times 10\right\}/24$	(8)
• $\text{USLE\_K} = \left\{0.2 + 0.3 \times e^{\left[-0.0256 \times \text{SOL\_SAND} \times \left(1 - \left(\frac{\text{SOL\_SILT}}{100}\right)\right)\right]}\right\} \times \left(\frac{\text{SOL\_SILT}}{\text{SOL\_CLAY}+\text{SOL\_SILT}}\right)^{0.3} \times \left[1 - \left(\frac{0.25 \times \text{SOL\_CBN}}{\text{SOL\_CBN} + e^{(3.72 - 2.95 \times \text{SOL\_CBN})}}\right)\right] \times \left[1 - \left(\frac{0.7 \times \text{SN1}}{\text{SN1} + e^{(-5.51 + 22.9 \times \text{SN1})}}\right)\right]$	(9)
○ $\text{SN1} = 1 - (\text{SOL\_SAND}/100)$	

Table 4. Pedotransfer models for bulk density (SOL_BD) and available water capacity (SOL_AWC). Table 1 contains the description of acronyms.

Saxton and Rawls (2006), SR	Eq.

- $\text{SOL\_BD} = \rho_B = \rho_N \times (1 - R_v) + (R_v \times 2.65)$ (10)
    - $\rho_N = (1 - \theta_S) \times 2.65$
        - $\theta_S = \theta_{33} + \theta_{(S-33)} - 0.097 \times (\text{SOL\_SAND}/100) + 0.043$
            - $\theta_{33} = \theta_{33t} + [1.283 \times (\theta_{33t})^2 - 0.374 \times (\theta_{33t}) - 0.015]$
                - $\theta_{33t} = -0.251 \times (\text{SOL\_SAND}/100) + 0.195 \times (\text{SOL\_CLAY}/100) + 0.011 \times \text{OM} + 0.006 \times [(\text{SOL\_SAND}/100) \times \text{OM}] - 0.027 \times [(\text{SOL\_CLAY}/100) \times \text{OM}] + 0.452 \times [(\text{SOL\_SAND}/100) \times (\text{SOL\_CLAY}/100)] + 0.299$
                    - $\text{OM} = \text{SOL\_CBN} \times 2$

                      As recommended (Pribyl, 2010).
            - $\theta_{(S-33)} = \theta_{(S-33)t} + \left(0.636 \times \theta_{(S-33)t} - 0.107\right)$
                - $\theta_{(S-33)t} = 0.278 \times (\text{SOL\_SAND}/100) + 0.034 \times (\text{SOL\_CLAY}/100) + 0.022 \times \text{OM} - 0.018 \times [(\text{SOL\_SAND}/100) \times \text{OM}] - 0.027 \times [(\text{SOL\_CLAY}/100) \times \text{OM}] - 0.584 \times [(\text{SOL\_SAND}/100) \times (\text{SOL\_CLAY}/100)] + 0.078$
    - $R_v = (\rho_R \times R_w)/[1 - R_w \times (1 - \rho_R)]$
        - $\rho_R = \rho_N/2.65$
        - $R_w = \text{SOL\_ROCK}/100$
- $\text{SOL\_AWC} = (\theta_{33} - \theta_{1500}) \times (1 - R_v)$ (11)
    - $\theta_{1500} = \theta_{1500t} + (0.14 \times \theta_{1500t} - 0.02)$
        - $\theta_{1500t} = -0.024 \times (\text{SOL\_SAND}/100) + 0.487 \times$

$(\mathrm{SOL\_CLAY}/100) + 0.006 \times \mathrm{OM} + 0.005 \times [(\mathrm{SOL\_SAND}/100) \times \mathrm{OM}] - 0.013 \times [(\mathrm{SOL\_CLAY}/100) \times \mathrm{OM}] + 0.068 \times [(\mathrm{SOL\_SAND}/100) \times (\mathrm{SOL\_CLAY}/100)] + 0.031$

Oliveira et al. (2006), OL

- $\mathrm{SOL\_BD} = f(\mathrm{SOL\_Z}) = \begin{cases} \mathrm{SOL\_BD}_{\leq 300}, \mathrm{SOL\_Z} \leq 300 \\ \mathrm{SOL\_BD}_{>300}, \mathrm{SOL\_Z} > 300 \end{cases}$ (12)
  - $\mathrm{SOL\_BD}_{\leq 300} = 1.5544 - 0.0004 \times (\mathrm{SOL\_CLAY} \times 10) - 0.01 \times (\mathrm{SOL\_CBN} \times 10) + 0.0067 \times (\mathrm{SB})$
  - $\mathrm{SOL\_BD}_{>300} = 1.5574 - 0.0005 \times (\mathrm{SOL\_CLAY} \times 10) - 0.006 \times (\mathrm{SOL\_CBN} \times 10) + 0.0076 \times (\mathrm{SB})$

Barros et al. (2013), BR

- $\mathrm{SOL\_AWC} = \theta_{33} - \theta_{1500}$ (13)
  - $\theta_{33} = \theta_r + \frac{\theta_s - \theta_r}{[1+(\alpha \times |\Psi|)^n]^m}$
    - $\theta_r = 0.0858 - 0.1671 \times (\mathrm{SOL\_SAND}/100) + 0.3516 \times (\mathrm{SOL\_CLAY}/100) + 1.1846 \times (\mathrm{OM}/100) + 0.000029 \times (\mathrm{SOL\_BD}/1000)$
    - $\theta_s = 1 - 0.00037 \times (\mathrm{SOL\_BD}/1000)$
    - $\alpha = 10^{\left[\begin{array}{c} 0.8118 + 0.8861 \times (\mathrm{SOL\_SAND}/100) - 1.1907 \times \\ (\mathrm{SOL\_CLAY}/100) - 0.001514 \times (\mathrm{SOL\_BD}/1000) \end{array}\right]}$
    - $n = 1.1527 + 0.7427 \times (\mathrm{SOL\_SAND}/100) + 0.4135 \times (\mathrm{SOL\_SILT}/100) - 5.5341 \times (\mathrm{OM}/100)$
    - $m = 1 - (1/n)$
    - $\Psi = 33$
  - $\theta_{1500} = \theta_r + \frac{\theta_s - \theta_r}{[1+(\alpha \times |\Psi|)^n]^m}$
    - $\Psi = 1500$

Oliveira et al. (2002), OL

- $\mathrm{SOL\_AWC} = \theta_{33} - \theta_{1500} =$ (14)

$$-0.000021 \times (\text{SOL\_SAND} \times 10) + 0.000203 \times (\text{SOL\_SILT} \times 10) + 0.000054 \times (\text{SOL\_CLAY} \times 10) + 0.021656 \times \text{SOL\_BD}$$

Tomasella et al. (2000), TM

- $\text{SOL\_AWC} = \theta_{33} - \theta_{1500}$ (15)
    - $\theta_{33} = \theta_r + \frac{\theta_s - \theta_r}{[1+(\alpha \times |\Psi|)^n]^m}$
        - $\theta_r = \begin{bmatrix} 23.3867 + 0.1103 \times \text{SOL\_CLAY} - 4.7949 \times \text{SOL\_BD} + \\ 0.0047 \times (\text{SOL\_SILT} \times \text{SOL\_CLAY}) - 0.0027 \times \text{CS}^2 - \\ 0.0022 \times \text{FS}^2 - 0.0048 \times \text{SOL\_SILT}^2 \end{bmatrix} \Big/ 100$
            - $\text{SOL\_SAND} = \text{CS} + \text{FS}$
        - $\theta_s = \begin{bmatrix} 91.6203 - 30.0046 \times \text{SOL\_BD} + 1.5925 \times \text{SOL\_CBN} + \\ 0.0022 \times (\text{CS} \times \text{SOL\_SILT}) - 0.0036 \times (\text{CS} \times \text{SOL\_CLAY}) - \\ 0.0018 \times \text{CS}^2 - 0.001 \times \text{FS}^2 \end{bmatrix} \Big/ 100$
        - $\alpha = e^{\left\{\begin{bmatrix} 205.6546 - 2.556 \times \text{SOL\_SILT} - 0.1329 \times \text{SOL\_CLAY} - 247.4904 \times \text{SOL\_BD} - \\ 0.0189 \times (\text{CS} \times \text{FS}) + 0.1177 \times (\text{CS} \times \text{SOL\_SILT}) + 0.0517 \times (\text{FS} \times \text{SOL\_CLAY}) + \\ 0.0617 \times \text{CS}^2 \end{bmatrix} \Big/ 100 \right\}}$
        - $n = \begin{pmatrix} 168.8617 - 0.0258 \times (\text{CS} \times \text{SOL\_SILT}) - \\ 0.0261 \times \big((\text{FS} \times \text{SOL\_CLAY})\big) + 0.0093 \times \text{FS}^2 - \\ 0.0077 \times \text{SOL\_SILT}^2 \end{pmatrix} \Big/ 100$
        - $m = 1 - (1/n)$
        - $\Psi = 33$
    - $\theta_{1500} = \theta_r + \frac{\theta_s - \theta_r}{[1+(\alpha \times |\Psi|)^n]^m}$
        - $\Psi = 1500$

2.9 Land-use data collection and spatial statistics

To exemplify one of the many potential applications using our results, we performed zonal statistics on the modeled soil textural attributes to analyze their distribution over multiple land-use types. For that, we acquired annual land-use maps from 1985 to 2019 via the API of the MAPBIOMAS project in the Google

Earth Engine (GEE; https://earthengine.google.com/). The MAPBIOMAS is an integrated initiative from Brazilian researchers to reconstruct land use and cover changes in Brazilian Biomes, using Landsat Archive and cloud computing capabilities (Souza et al., 2020). They were able to map forest and non-forest natural formation, farming, non-vegetated areas, and water bodies for the entire country at high spatial resolution (30 m). The overall accuracy of the final MAPBIOMAS product is 89% (Souza et al., 2020). Detailed tutorials on how to acquire all data can be found at https://mapbiomas.org/.

To analyze differences in soil texture among distinct land-use classes, we first submitted all 35 maps to an intercept geoprocessing tool in the package QGIS 3.10.3 (downloadable at https://qgis.org/), producing a raster where its pixels reflect the areas where no changes in land use occurred during the 1985–2019 period, i.e., zonal raster. Then, we used this zonal raster to acquire spatial statistics of the soil texture attributes per land use class.

3 Results and discussion

3.1 Model approximation

The spatial modeling produced 64,415 patches with an average area of 1.35 ± 4.54 km^2, and an average density of 0.75 patches per km^2. Each one of these were considered as a virtual soil profile for which GBM outputs were calculated. When working with DSM, having a high level of model predictive ability is essential because of the inductive nature of the soil mapping science, where patterns in observations are found and declared to be a general model (Overmars et al., 2007). However, preventing overfitting is important due to the nature of successive boosting inherent in GBMs, which allows decision trees to be added until the model is completely overfitted (Dormann et al., 2007). To avoid this from happening, the structure of the trees must be tuned by adjusting the models hyperparameters. This structure is usually calibrated by applying a calibration algorithm with a range of possible values for each hyperparameter ($b_{i,min}$–$b_{i,max}$). In this study, the models demonstrated a consistent ability to perform such extrapolations as the performance of the models during the verification were similar to those found by the calibration algorithm (Table 5). The r^2 and PBIAS values varied from 0.79 to 0.98, and from -1.39 to 1.14, respectively. Among all models for textural properties, the lowest r^2 value was found for the modeled SOL_SILT (0.79). We believe that the large number of predictors, each with similar importance, for the SOL_SILT model (Table 5) may have caused prediction redundancies, and probably degraded the model strength by increasing its variance, even though we applied a RFS algorithm for feature selection.

When comparing descriptive statistics between the simulated and observed reference datasets, differences are expected since the observed dataset was not created using a systematic sampling, thus there are spaces with singular environmental properties that were not captured in our observed dataset. The highest differences were found for SOL_ROCK (44.5%), SB (53.1%), CS (103.3%) and FS (31.9%). Even without a systematic sampling approach, these values should not be excessively high since the observed dataset still covers the entire study area and a high diversity of environments (Table 6). We attribute these high differences in SOL_ROCK to the calculation of the parameter as a residual of all textural parameters, which was not directly modeled. As for CS and FS, they were directly modeled but unavoidably resampled to a total of 100%. We did not use the same technique for the texture parameters, and choose to sacrifice SOL_ROCK prediction accuracy, because its spatial variance produces a high number of zeros (38.5% of the total values) in comparing to all other parameters (< 0.01%), leaving not enough variance to perform any modeling accurately. Although SB exhibited no zeros in the dataset, it produced a similar effect on regressors as SOL_ROCK did because 21.98% of its values ranged between 0.1 and 3.84 $cmol_c$ kg^{-1}, presenting an exponential data distribution. Finally, 51.49% of the 135,934 virtual profiles exhibited some uncertainty. Most of the uncertainty was under 15% and its highest value was of 51.49% (Fig. 6).

Table 5. Calibrated values for the hyperparameters n_estimators (NE), max_depth (MD), min_samples_split (MSS) and min_samples_leaf (MSL) of the Gradient Boosting Models (GBM) of basic soil properties, and their calibration performance. The description of the variables can be found in Table 1.

Output	Calibrated hyperparameters				Calibration	Verification		
	NE	MD	MSS	MSL	Accuracy[(a)] or $r^{2(b)}$	Accuracy[(a)] or $r^{2(b)}$	RMSE	PBIAS
L_MAX	1325	23	41	70	0.91[(a)]	0.96[(a)]	-	-
SOL_Z (mm)	4445	3	36	7	0.92[(b)]	0.98[(b)]	73.19	0.02
SOL_SAND (%)	2521	87	73	6	0.77[(b)]	0.91[(b)]	6.27	1.14
SOL_CLAY (%)	1518	38	85	12	0.78[(b)]	0.93[(b)]	4.48	0.29
SOL_SILT (%)	1624	85	15	3	0.76[(b)]	0.79[(b)]	4.77	-1.36
SOL_CBN (%)	1265	27	17	43	0.78[(b)]	0.91[(b)]	0.14	-3.39
SB ($cmol_c$ kg^{-1})	1026	46	23	2	0.82[(b)]	0.95[(b)]	1.79	2.97
CS (%)	2893	38	40	63	0.92[(b)]	0.98[(b)]	2.46	1.04
FS (%)	2282	3	7	13	0.89[(b)]	0.97[(b)]	2.03	-0.03

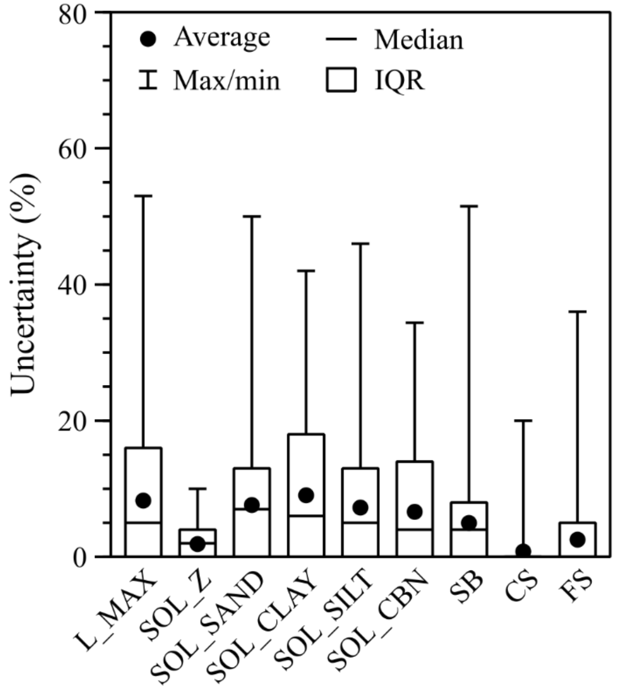

Figure 6: Uncertainty analysis of the Gradient Boosting Models (GBM) of the basic soil parameters for the estimates whose inputs extrapolated the calibration range of values. The description of the variables can be found in Table 1.

Table 6. Descriptive statistics of the 18 Gradient Boosting Models of basic soil properties, with the reference observed values between parentheses. The description of the variables can be found in Table 1.

Basic property	Mean±SD		Minimum		Maximum	
L_MAX	4±1	(4±1)	1		(1)	
SOL_Z (mm)	700.88±475.26	(737.36±559.63)	1	(50)	8	(8)
SOL_SAND (%)	46.77±13.08	(51.52±21.27)	0	(0)	3051.4	(2550)
SOL_CLAY (%)	28.87±11.7	(27.3±17.51)	0	(0)	97.09	(98)
SOL_SILT (%)	17.99±6.4	(16.78±10.67)	0	(0)	83.6	(83.6)
SOL_ROCK (%)	6.37±7.89	(4.41±10.63)	0	(0)	56.92	(59)

SOL_CBN (%)	0.58±0.36	(0.54±0.49)	0.0002	(0)	100	(100)
SB ($cmol_c$ kg^{-1})	10.67±7.76	(6.97±8.39)	0.01	(0.14)	3.38	(3.38)
CS (%)	67.96±9.66	(29.51±18.46)	0	(0)	46.11	(49.74)
FS (%)	32.03±9.65	(24.28±13.09)	0	(0.4)	100	(88)

Reference observed values within parentheses.

3.2 Environmental modulators

Results showed that the soil properties were relatively sensitive to climate, topographic, and vegetation properties (Fig. 7). Understanding how these environmental factors affect the physical and chemical soil properties can support the management of their changes in response to future climate conditions or deforestation (Badía et al., 2016). In our study area, the properties related to topographic and climatic conditions were dominating when estimating all attributes, whereas the properties regarding vegetation were especially strong for the soil property estimates related to sand, i.e., SOL_SAND, CS and FS. Topography is always present as input variables in our models (Table 7), and it is indeed an important factor in soil formation in Northeast Brazil (Oliveira et al., 2018). The topographic conditions can be divided into the slope, which may affect the quantity of soil deposition or erosion; the aspect, which drives the water flux direction over the soils, and relative exposure of the soils to sunlight; and the curvature, which changes flow velocity, controlling the erosion and deposition processes (Patton et al., 2018; Barbieri et al., 2009).

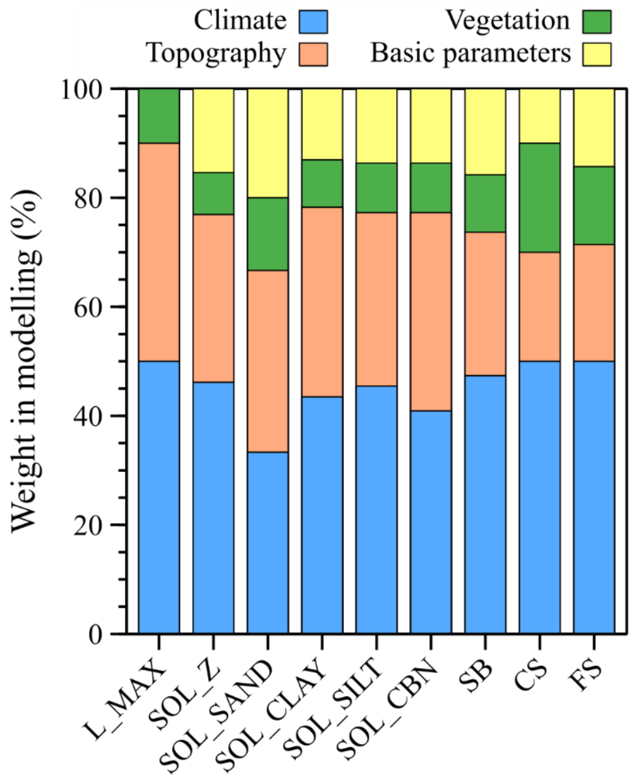

Figure 7: Proportional weights (w, as in Eq. (6)) of the different types of inputs for modeling each basic soil parameter. The description of the variables can be found in Table 1.

Table 7. List of input parameters used for calibrating the Gradient Boosting Models of basic soil properties. The weights (w) calculated for each input in the models are between parentheses. The description of the variables and parameters can be found in Table 1.

Output	Inputs
L_MAX	NDVI (0.18), DEM (0.13), ASPECT (0.07), PCPMM (0.07), WNDAV (0.07), AAT_ASPECT (0.05), CUR (0.05), TMPSTDMX (0.05), TMPMX (0.04), ATT_CUR (0.03), CTI (0.03), SPR (0.03), PCPSTD (0.03), TMPMN (0.03), TMPSTDMN (0.03), ATT_SPR_F (0.02), LST (0.02), PCPSKW (0.02), DEWPT (0.02), SOLARAV (0.02).

SOL_Z	LAYER (0.83), AAT_ASPECT (0.02), CUR (0.02), NDVI (0.02), DEM (0.02), TMPMN (0.02), L_MAX (0.02), CTI (0.01), PCPSKW (0.01), PCPMM (0.01), SOLARAV (0.01), WNDAV (0.01), TMPSTDMN (0.01).
SOL_SAND	NDVI (0.09), WNDAV (0.09), CTI (0.08), LST (0.08), SOL_Z (0.08), ASPECT (0.07), CUR (0.07), TMPMN (0.07), PCPSKW (0.06), DEM (0.06), LAYER (0.06), ATT_CUR (0.05), TMPMX (0.05), TMPSTDMN (0.05), L_MAX (0.05).
SOL_CLAY	AAT_ASPECT (0.08), PCPMM (0.08), LST (0.07), ASPECT (0.06), CUR (0.06), WNDAV (0.06), DEM (0.05), CTI (0.04), NDVI (0.04), PCPSTD (0.04), ATT_CUR (0.03), DEWPT (0.02), SOLARAV (0.02), TMPSTDMX (0.02), TMPMN (0.02), TMPSTDMN (0.02), ATT_SPR_F (0.01), SPR (0.01), PCPSKW (0.01), TMPMX (0.01).
SOL_SILT	TMPMN (0.11), SOL_Z (0.1), DEM (0.09), ASPECT (0.07), PCPMM (0.07), CTI (0.05), CUR (0.05), DEWPT (0.05), L_MAX (0.05), AAT_ASPECT (0.04), ATT_SPR_F (0.04), NDVI (0.04), SOLARAV (0.03), TMPSTDMX (0.03), TMPSTDMN (0.03), LAYER (0.03), SPR (0.02), LST (0.02), WNDAV (0.02), TMPMX (0.02), PCPSKW (0.01), PCPSTD (0.01).
SOL_CBN	LAYER (0.24), SOL_Z (0.2), ATT_CUR (0.07), NDVI (0.06), CUR (0.04), WNDAV (0.04), AAT_ASPECT (0.03), CTI (0.03), SPR (0.03), PCPSKW (0.03), PCPSTD (0.03), PCP_MM (0.03), DEM (0.03), ASPECT (0.02), ATT_SPR_F (0.02), LST (0.02), SOLARAV (0.02), TMPMN (0.02), TMPSTDMN (0.02), L_MAX (0.02), DEWPT (0.01), TMPSTDMX (0.01).
SB	DEWPT (0.19), WNDAV (0.14), PCPSTD (0.08), DEM (0.07), SOL_Z (0.07), TMPMN (0.06), LST (0.05), TMPSTDMX (0.05), ASPECT (0.04), CUR (0.04), PCPMM (0.04), L_MAX (0.04), AAT_ASPECT (0.03), TMPSTDMN (0.03), NDVI (0.02), LAYER (0.02), ATT_CUR (0.01), SOLARAV (0.01), TMPMX (0.01).
CS	SOL_SAND (0.65), TMPSTDMX (0.06), DEM (0.05), TMPMX (0.05), SPR

	(0.04), LST (0.04), NDVI (0.04), SOLARAV (0.03), WNDAV (0.03), PCPSTD (0.02).
FS	SOL_SAND (0.4), SOLARAV (0.09), NDVI (0.07), ATT_CUR (0.05), SPR (0.05), DEM (0.05), TMPMX (0.05), TMPSTDMX (0.05), LST (0.04), PCPMM (0.04), DEWPT (0.03), TMPSTDMN (0.03), SOL_Z (0.03), WNDAV (0.02).

Our model for SB was mainly influenced by relative air humidity (19%) and wind speed (14%). These variables are known for controlling the intensity of biochemical reactions, and wind erosion (Ravi et al., 2004), and are capable of moving nutrients and thus affect its local content. Although precipitation may be an important climate driver in other regions, e.g., Dixon et al. (2016), its characteristics, i.e., PCPSTD and PCPMM, counted only for 12% of our model for SB, and the low r^2 (0.34) between DEWPT and PCPMM suggests that relative air humidity was not used due to its potential, although non-existent, strong correlation to rainfall. At high relative humidity, soil chemicals weather relatively quickly, and this is an extremely favorable condition to biochemical reactions, which may increase the yields of organic matter, and limit the partitioning of organic chemicals into the soil (Truu et al., 2017; Eppes et al., 2020). In addition, air humidity affects erosion, as soil particles may become more aggregated. This is explained by the effect of hygroscopic forces and their dependence on soil matric potential, especially in dry soils (Davarzani et al., 2014; Ravi et al., 2004). For the wind speed, it may change the contents of topsoil nutrients (Zobeck et al., 1989), especially in arid and semi-arid regions, as seen in the west region of our study area, where soils are dry and covered by a sparse vegetation (Ravi et al., 2004).

The L_MAX model had NDVI (18%) and terrain elevation (13%) as its main inputs. Although the elevation is a topographic variable, it often modulates climate conditions as it is related to physical features that may create ‘climate islands’ (Badía et al., 2016), either by the processes of rain shadows or via changes on atmospheric lapse rates (Nettesheim et al., 2015). Thus, it is well related to meteorological conditions (Badía et al., 2016), which impact the speed at which parent materials weather, and hence the rate of soil development. As for NDVI, it reflects indirectly the vertical variability in the soil, as soils formed under forests tend to be more weathered. It happens because forests grow in higher rainfall areas (Bonan, 2008).

Other model inputs include CTI and the basic parameters themselves, which, in our case, are L_MAX, SOL_Z and SOL_SAND. CTI is especially important when predicting various soil properties, as it encapsulates the terrain structure (Moore et al., 1993; Gessler et al., 1995, 2000; Ziadat, 2010). The SOL_SAND and SOL_SILT estimates were strongly modulated by the SOL_Z. Sand formation is well reported to occur on top layers that are more vulnerable to all types of erosion (Das and Deka, 2020). Silt content variations are mainly driven by the temperature profile in the soil that affects soil aeration though changes in producing CO_2, and soil structure by modulating interactions among the clay particles, yielding less clay and more silt in deeper layers. The SOL_SAND also showed a moderate relationship with the vegetation inputs. The vegetation cover is a potential indicator of weathered soils, or reduced sand contents, as soils formed under dense forests are usually in high-rainfall areas (Souza et al., 2016), as seen the eastern region of our study area.

3.3 Hydraulic parameters

The moist bulk density estimates SOL_BD_{SR} (Saxton and Rawls, 2006) and SOL_BD_{OL} (Oliveira et al., 2006) were similar, with mean differences of only 0.11 g cm^{-3} (Table 8). These models produced an acceptable range of values since other studies in Brazil have found a maximum variation between 0.13 and 2.25 g cm^{-3}, e.g., Benites et al. (2007) and Boschi et al. (2018). In general, PTFs tend to be over-adjusted, to varying degrees, to the dataset used in their calibration step (De Vos et al., 2005). For the SOL_AWC, SOL_AWC_{OL}, which was calibrated strictly using data from Pernambuco State, was the only equation that did not saturate when simulations were performed (Oliveira et al., 2006). As we evaluate and map soils for a common region to Oliveira et al. (2006), these results highlight the overfitting trend that usually exists in PTFs.

Table 8. Descriptive statistics of all calculated pedotransfer functions (PTF) data using basic soil properties derived from Gradient Boosting Models (GBM).

PTF outputs	Mean (SD)	Minimum	Maximum	Invalid values (%)
SOL_BD_{SR} (g cm^{-3})	1.54 (0.09)	1.01	2.23	0
SOL_BD_{OL} (g cm^{-3})	1.45 (0.07)	1.12	1.76	0
SOL_AWC_{SR} (mm mm^{-1})	0.11 (0.01)	0.01	0.18	0
SOL_AWC_{BR} (mm mm^{-1})	0.05 (0.03)	0.001	0.17	0.75
SOL_AWC_{TM} (mm mm^{-1})	0.03 (0.01)	0.001	0.13	5.01
SOL_AWC_{OL} (mm mm^{-1})	0.07 (0.01)	0.01	0.16	0
SOL_K_{SR} (mm hr^{-1})	11.17 (14.24)	0.003	932.54	0
$SOL\_K_{SR/BR}$ (mm hr^{-1})	1101.28 (350.5)	10.41	1900.21	0
$SOL\_K_{SR/TM}$ (mm hr^{-1})	26.72 (26.58)	0.001	219.47	12.07
SOL_K_{BK} (mm hr^{-1})	63.85 (333.9)	8.85	12112	0
USLE_K	0.22 (0.03)	0.01	0.41	0

Two of the four estimates of SOL_K were variations of the equation described in Saxton and Rawls (2006). The difference between them is in the calculation of the inputs θ_S, θ_{33} and θ_{1500}, which differs from the one originally proposed by Saxton and Rawls (2006), SOL_K_{SR} to the approaches of Barros et al. (2013), SOL_K_{BR}, and Tomasella et al. (2000), SOL_K_{TM}. Maximum values ranged from 219.47 ($SOL\_K_{SR/TM}$) to 12,112 mm h^{-1} (SOL_K_{BK}). The SOL_K_{BK} is the simplest approach. It has only the SOL_Z as input, and therefore it reflects only a fixed range of soil textures. Invalid values were observed only for $SOL\_K_{SR/TM}$ due to saturations of θ_r and n, which produced negative values and exponents in the model. For USLE_K, the applied model expects values varying from 0.1 to 0.5 (Sharpley and Williams, 1990), but we reached values below this threshold. This happened because our simulated dataset presents soils with high coarse-sand contents.

The models developed in this study used a dataset of *in situ* observations from a range of different climates, vegetation covers and slope conditions. This dataset produced the variance required by the GBM; and was a key element to apply the framework successfully. When applying these methods to other regions, we recommend performing a simple dataset splitting test to evaluate whether the models are being fed with an appropriate (*i*) number of samples, and (*ii*) quality dataset, i.e., whether it has sufficient variance. Normally, the model performance is not heavily affected by an increase in the number of samples in a dataset, as it prevents corruption of its variance. However, if the sample size is small — this is region-specific and can be only evaluated by performing tests — the overall variance will be easily impacted by individual samples. In this study, we selected the input parameters based on their known soil forming relationship, as we are doing an analysis over the soil modulators; but this is not strictly required to reproduce this methodology for other regions. Multiple variations of a single parameter can be applied as long as it does not violate the assumption of multi-collinearity.

3.4 Land cover types and soil texture linkages

Our results show a predominance of high sandy content with a higher density of points exhibiting a 40–70% content for sandy, followed by 20–45% for clay, and 15–25% for silt (Fig. 8). The highest clay content values were found in the East of the Pernambuco State region, covering an area extending from about 20 to 100 km from the coast (Fig. 9). For the remaining area, the sand content is approximately twice higher, and the highest silt content is found within the transition of high clay to sandy areas. There are a few coarse sand-dominated soil patches in sedimentary basins, such as the Jatobá, Belmonte and Fátima, in coastal lowlands, and smaller portions in the coastal plateaus close to the Atlantic Ocean. Moreover, in the West of the study area, there are sandy surface layers at the top of the Araripe plateau.

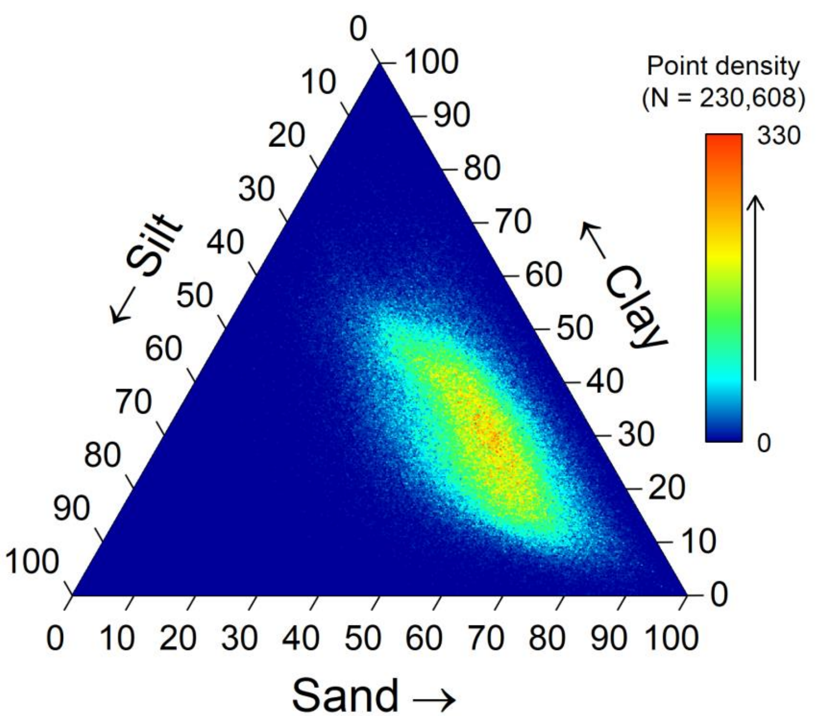

Figure 8: Modeled soil textural distribution for sand, silt and clay.

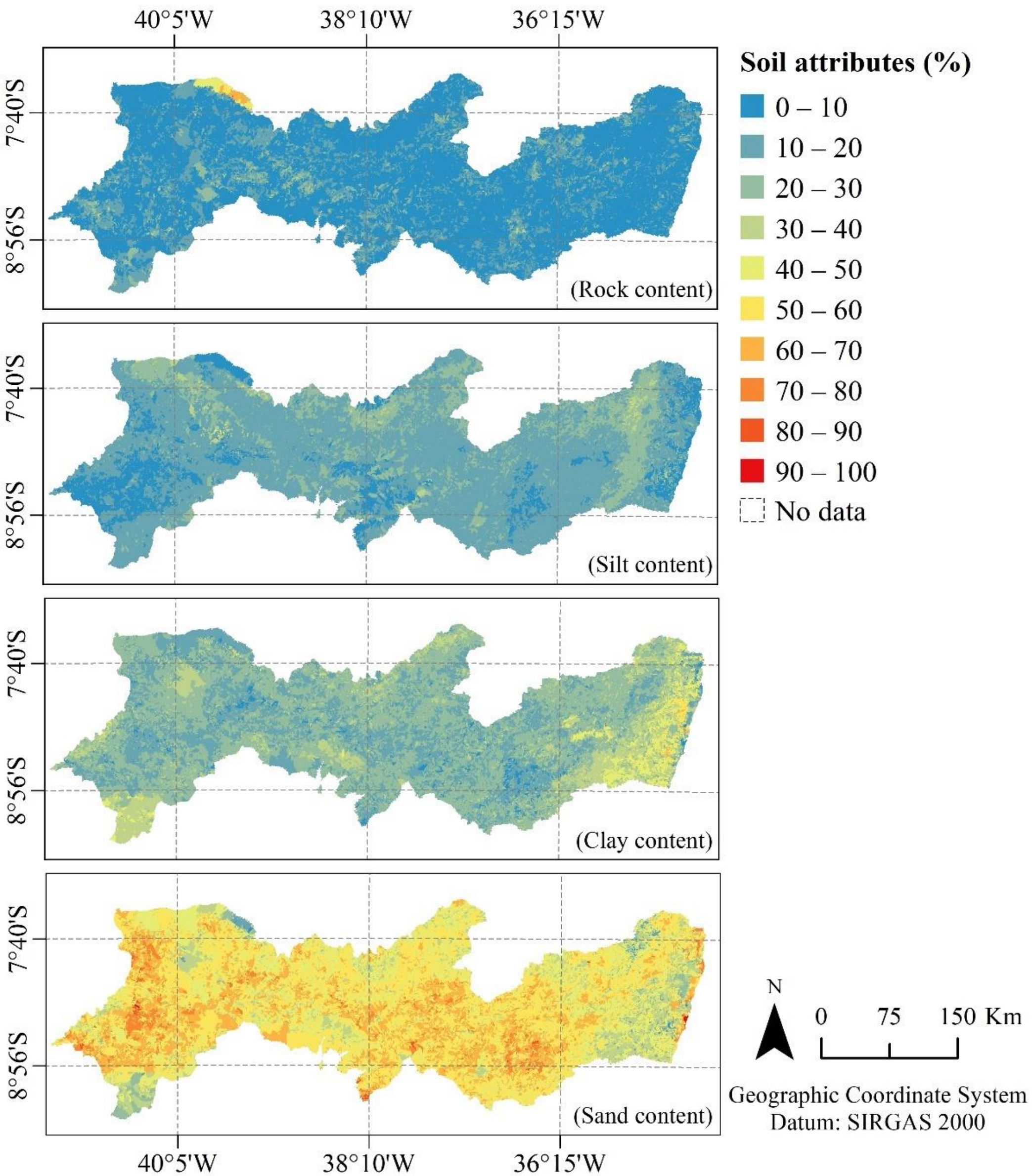

Figure 9: Maps of the modeled soil texture attributes over the study area.

Not surprisingly, the soils with the highest clay content are covered with agricultural fields (Fig. 10) since higher soil water retention is expected as soils particle distribution gets finer (Newman, 1984). Over these patches of higher clay content, agriculture practices vary across the study area due to contrasting precipitation patterns. In the East, the precipitation is the highest and water-intensive sugar cane plantations are predominant over the areas with the highest clay content (38.9% ± 10.6%). In the Southernmost part of our study area, where the climate is dry with low precipitation rates, there is a region with relatively high clay content (over 30%) known as the São Francisco Valley; there, perennial crops are maintained via irrigation systems supplied with water from the San Francisco River, which crosses the valley.

We found that approximately 50% of the entire study area had at least one type of land-cover conversion over the 1985–2019 period. The joint analysis of land-use changes and high-resolution robust soil mapping is only one of the applications that is possible with the use of the methodology we propose. For example, since the expansion of agriculture has been towards areas with higher clay content, our results can support the development of strategic plans to improve the use of poorly managed areas with high clay content. Moreover, our maps can be used as evidence in support of environmental policies to prioritize the protection of native vegetation in clayey soils that are particularly vulnerable to deforestation.

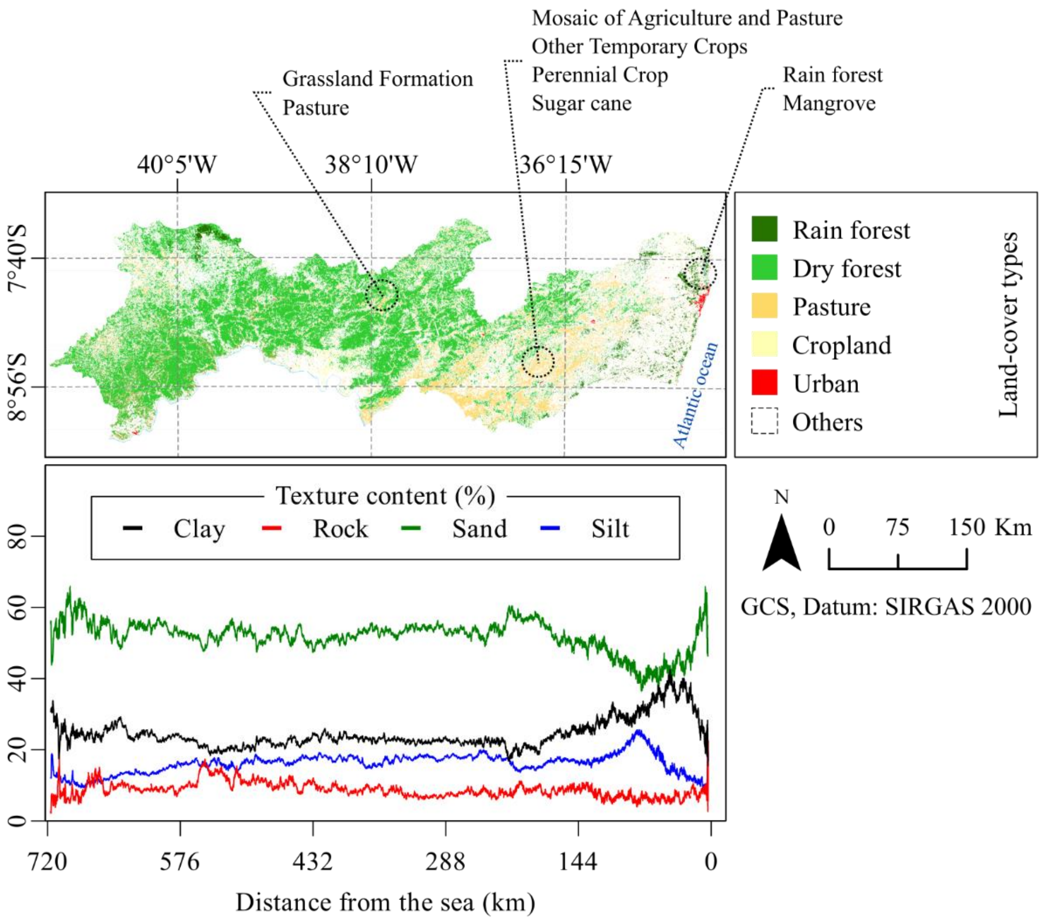

Figure 10: Modeled soil texture attributes and land-cover across the study area.

4 Conclusions

In this study we produced a robust soil map using inductive ML techniques based on decision trees for the highly variable Pernambuco State region in Brazil. The good quality of the overall model performance is reflected in our models' statistics that presents r^2 and PBIAS values varying from 0.79 to 0.98, and from -1.39 to 1.14, respectively. The advantage of decision tree methods can be far greater than classical linear regression because decision tree methods are entirely free of strict assumptions, and all types of variables, scales, distributions, and relations can be jointly handled at once. We explored this characteristic in detail in this study, by employing multiple freely available datasets with an extensive range of data types (e.g., the number of soil layers and chemical composition) to improve the soil information in our study area. Although GBM may be considered semi-black-box models, adding a feature selector in the calibration processing allowed us to perform uncertainty analyses and pinpoint the main environmental modulators of different soil properties.

Our results are especially important for soil management in response to climate change or land use and land management changes, such as deforestation and desertification, at multiple spatial scales. The novel hybrid machine learning framework includes enhanced flexibility, the possibility of producing regular short-term map updates, and supporting future economic and environmental modeling integration (e.g., https://super.hawqs.tamu.edu/), while drastically reducing capital investments compared to *in situ* surveys and mapping. We believe that these promising findings will improve all soil-related modeling efforts and will encourage the development of new framework and datasets for soil sciences. Our new dataset can be further used to create a new portfolio of applications for soil science, innovative research, agricultural zoning, and environmental management strategies.

Acknowledgments

Soil data was provided by the Brazilian Agricultural Research Corporation (EMBRAPA) through the Agroecological Zoning of the state of Pernambuco (ZAPE) project. The authors also acknowledge the following funding sources: The Brazilian Coordination for the Improvement of Higher Level Personnel (CAPES 88887.371850/2019-00) for AGSSS and JDG; The Fundação de Amparo a Ciência e Tecnologia do Estado de Pernambuco (Project FACEPE APQ, 0646-9.25/16) for RQM and JDG; The National Council for Scientific and Technological Development of Brazil (CNPq) through the projects MCTIC/CNPq 28/2018 (431980/2018-7), PEGASUS MCTI/CNPq Nº 19/2017 (441305/2017-2), CNPq/MCTIC/BRICS 29/2017 (442335/2017.2), INCT Mudanças Climáticas II, and productivity grants (448236/2014-1 and 313469/2020-2) for SMGLM; and the UK Natural Environment Research Council (NE/N012526/1 ICL and NE/N012488/1 UoR) and FAPESP (The São Paulo Research Foundation) (FAPESP 2015/50488-5) for the UK/Brazil Nordeste project for AV, RLBN and MSBM.

Code availability

The code developed and used in this study is freely available at the GitHub repository (https://github.com/razeayres/sleepy).

Data availability

The datasets generated and analyzed in this study are available at the Zenodo repository (https://zenodo.org/record/5918544). The observed data used to support the findings of this study comes from the Agroecological Zoning of the state of Pernambuco (ZAPE) project of the Brazilian Agricultural Research Corporation (EMBRAPA), it is not licensed for redistribution and it can be acquired by contacting the Soil Unit of EMBRAPA at cnps.sac@embrapa.br.

Author contribution

Conceptualization: RQM, RLBN and JDG; Data curation: RQM, ELRS, JCAF, AHCB and RLBN; Formal Analysis: RQM, RLBN, AGSSS and JDG; Investigation: RQM, RLBN, MSBM and JDG; Methodology: RQM, RLBN, JFS, MSBM, FZ, AV and JDG; Project administration: RQM and JDG; Resources: JDG; Software: RQM, RLBN and JDG; Validation: RQM, RLBN, AV and MSBM; Visualization: RQM, RLBN, AV, MSBM and MSBA; Writing – original draft: all authors; Writing – review & editing: all authors.

References

ABNT: NBR 6502: Rocks and soils - Terminology, 1995.

Adhikari, K., Hartemink, A. E., Minasny, B., Bou Kheir, R., Greve, M. B., and Greve, M. H.: Digital Mapping of Soil Organic Carbon Contents and Stocks in Denmark, 9, e105519, https://doi.org/10.1371/journal.pone.0105519, 2014.

Akpa, S. I. C., Odeh, I. O. A., Bishop, T. F. A., Hartemink, A. E., and Amapu, I. Y.: Total soil organic carbon and carbon sequestration potential in Nigeria, 271, 202–215, https://doi.org/10.1016/j.geoderma.2016.02.021, 2016.

Alvares, C. A., Stape, J. L., Sentelhas, P. C., de Moraes Gonçalves, J. L., and Sparovek, G.: Köppen's climate classification map for Brazil, 22, 711–728, https://doi.org/10.1127/0941-2948/2013/0507, 2013.

Araújo Filho, J. C., Burgos, N., Lopes, O. F., Silva, F. H. B. B. Da, Medeiros, L. A. R., Melo Filho, H. F. R. De, Parahyba, R. D. B. V., Cavalcanti, A. C., Oliveira Neto, M. B. De, Silva, F. B. R. E., Leite, A. P., Santos, J. C. P. Dos, Souza Neto, N. C. De, Silva, A. B. Da, Luz, L. R. Qu. P. Da, Lima, P. C. De, Reis, R. M. G., and Barros, A. H. C.: Levantamento de reconhecimento de baixa e média intensidade dos solos do Estado de Pernambuco, Boletim de Pesquisa N 11, 382 pp., 2000.

Arnold, J. G., Srinivasan, R., Muttiah, R. S., and Williams, J. R.: Large area hydrologic modeling and assessment. Part I: model development, 34, 73–89, https://doi.org/10.1111/j.1752-1688.1998.tb05961.x, 1998.

Badía, D., Ruiz, A., Girona, A., Martí, C., Casanova, J., Ibarra, P., and Zufiaurre, R.: The influence of elevation on soil properties and forest litter in the Siliceous Moncayo Massif, SW Europe, 13, 2155–2169, https://doi.org/10.1007/s11629-015-3773-6, 2016.

Ballabio, C., Panagos, P., and Monatanarella, L.: Mapping topsoil physical properties at European scale using the LUCAS database, 261, 110–123, https://doi.org/10.1016/j.geoderma.2015.07.006, 2016.

Barbieri, D. M., Marques Júnior, J., Alleoni, L. R. F., Garbuio, F. J., and Camargo, L. A.: Hillslope curvature, clay mineralogy, and phosphorus adsorption in an Alfisol cultivated with sugarcane, 66, 819–826, https://doi.org/10.1590/S0103-90162009000600015, 2009.

Barros, A. H. C., Lier, Q. D. J. Van, Maia, A. de H. N., and Scarpare, F. V.: Pedotransfer functions to estimate water retention parameters of soils in northeastern Brazil, 37, 379–391, https://doi.org/10.1590/S0100-06832013000200009, 2013.

Beguería, S., Spanu, V., Navas, A., Machín, J., and Angulo-Martínez, M.: Modeling the spatial distribution of soil properties by generalized least squares regression: Toward a general theory of spatial variates, 68, 172–184, https://doi.org/10.2489/jswc.68.3.172, 2013.

Behrens, T., Schmidt, K., Viscarra Rossel, R. A., Gries, P., Scholten, T., and MacMillan, R. A.: Spatial modelling with Euclidean distance fields and machine learning, 69, 757–770, https://doi.org/10.1111/ejss.12687, 2018.

Belk, E. L., Markewitz, D., Rasmussen, T. C., Carvalho, E. J. M., Nepstad, D. C., and Davidson, E. A.: Modeling the effects of throughfall reduction on soil water content in a Brazilian Oxisol under a moist tropical forest, 43, 1–14, https://doi.org/10.1029/2006WR005493, 2007.

Benites, V. M., Machado, P. L. O. A., Fidalgo, E. C. C., Coelho, M. R., and Madari, B. E.: Pedotransfer functions for estimating soil bulk density from existing soil survey reports in Brazil, 139, 90–97, https://doi.org/10.1016/j.geoderma.2007.01.005, 2007.

Best, M. J., Pryor, M., Clark, D. B., Rooney, G. G., Essery, R. . L. H., Ménard, C. B., Edwards, J. M., Hendry, M. A., Porson, A., Gedney, N., Mercado, L. M., Sitch, S., Blyth, E., Boucher, O., Cox, P. M., Grimmond, C. S. B., and Harding, R. J.: The Joint UK Land Environment Simulator (JULES), model description – Part 1: Energy and water fluxes, 4, 677–699, https://doi.org/10.5194/gmd-4-677-2011, 2011.

Bonan, G. B.: Forests and Climate Change: Forcings, Feedbacks, and the Climate Benefits of Forests, 320, 1444–1449, https://doi.org/10.1126/science.1155121, 2008.

Boschi, R. S., Bocca, F. F., Lopes-Assad, M. L. R. C., and Assad, E. D.: How accurate are pedotransfer functions for bulk density for Brazilian soils?, 75, 70–78, https://doi.org/10.1590/1678-992x-2016-0357, 2018.

Bossa, A. Y. Y., Diekkrüger, B., Igué, A. M. M., and Gaiser, T.: Analyzing the effects of different soil databases on modeling of hydrological processes and sediment yield in Benin (West Africa), 173–174, 61–74, https://doi.org/10.1016/j.geoderma.2012.01.012, 2012.

Bouma, J. and McBratney, A.: Framing soils as an actor when dealing with wicked environmental problems, 200–201, 130–139, https://doi.org/10.1016/j.geoderma.2013.02.011, 2013.

Chawla, N. V, Bowyer, K. W., Hall, L. O., and Kegelmeyer, W. P.: SMOTE : Synthetic Minority Over-sampling Technique, 16, 321–357, https://doi.org/https://doi.org/10.1613/jair.953, 2002.

Clark, D. B., Mercado, L. M., Sitch, S., Jones, C. D., Gedney, N., Best, M. J., Pryor, M., Rooney, G. G., Essery, R. L. H., Blyth, E., Boucher, O., Harding, R. J., Huntingford, C., and Cox, P. M.: The Joint UK Land Environment Simulator (JULES), model description – Part 2: Carbon fluxes and vegetation dynamics, 4, 701–722, https://doi.org/10.5194/gmd-4-701-2011, 2011.

Das, I. and Deka, S.: Application of rom scale for estimating bank erosion vulnerable areas in Kamrup district, Assam, 11, 1652–1656, https://doi.org/10.34218/IJM.11.12.2020.151, 2020.

Davarzani, H., Smits, K., Tolene, R. M., and Illangasekare, T.: Study of the effect of wind speed on evaporation from soil through integrated modeling of the atmospheric boundary layer and shallow subsurface, 50, 661–680, https://doi.org/10.1002/2013WR013952, 2014.

Davie-Martin, C. L., Hageman, K. J., Chin, Y.-P., Rougé, V., and Fujita, Y.: Influence of Temperature, Relative Humidity, and Soil Properties on the Soil–Air Partitioning of Semivolatile Pesticides: Laboratory Measurements and Predictive Models, 49, 10431–10439, https://doi.org/10.1021/acs.est.5b02525, 2015.

Dixon, J. L., Chadwick, O. A., and Vitousek, P. M.: Climate-driven thresholds for chemical weathering in postglacial soils of New Zealand, 121, 1619–1634, https://doi.org/10.1002/2016JF003864, 2016.

Dormann, C. F., McPherson, J. M., Araújo, M. B., Bivand, R., Bolliger, J., Carl, G., Davies, R. G., Hirzel, A., Jetz, W., Daniel Kissling, W., Kühn, I., Ohlemüller, R., Peres-Neto, P. R., Reineking, B., Schröder, B., M. Schurr, F., and Wilson, R.: Methods to account for spatial autocorrelation in the analysis of species distributional data: a review, 30, 609–628, https://doi.org/10.1111/j.2007.0906-7590.05171.x, 2007.

Elith, J., Leathwick, J. R., and Hastie, T.: A working guide to boosted regression trees, 77, 802–813, https://doi.org/10.1111/j.1365-2656.2008.01390.x, 2008.

Ellili-Bargaoui, Y., Malone, B. P., Michot, Di., Minasny, B., Vincent, S., Walter, C., and Lemercier, B.: Comparing three approaches of spatial disaggregation of legacy soil maps based on the Disaggregation and Harmonisation of Soil Map Units Through Resampled Classification Trees (DSMART) algorithm, 6, 371–388, https://doi.org/10.5194/soil-6-371-2020, 2020.

EMBRAPA: Manual de métodos de análise de solo, 2nd ed., Embrapa-CNPS, Rio de Janeiro, BRA, 212 pp., 1997.

Eppes, M. C., Magi, B., Scheff, J., Warren, K., Ching, S., and Feng, T.: Warmer, Wetter Climates Accelerate Mechanical Weathering in Field Data, Independent of Stress-Loading, 47, https://doi.org/10.1029/2020GL089062, 2020.

Esfandiarpour-Boroujeni, I., Shahini-Shamsabadi, M., Shirani, H., Mosleh, Z., Bagheri-Bodaghabadi, M., and Salehi, M. H.: Assessment of different digital soil mapping methods for prediction of soil classes in the Shahrekord plain, Central Iran, 193, 104648, https://doi.org/10.1016/j.catena.2020.104648, 2020.

Filho, J. C. de A., Araújo, M. do S. B. de, Marques, F. A., and Lopes, H. L.: SOLOS, in: Geodiversidade do estado de Pernambuco, edited by: Torres, F. S. de M. and Pfaltzgraff, P. A. dos S., CPRM, Recife, BRA, 109–138, 2014.

van Genuchten, M. Th.: A Closed-form Equation for Predicting the Hydraulic Conductivity of Unsaturated Soils, 44, 892–898, https://doi.org/10.2136/sssaj1980.03615995004400050002x, 1980.

Gessler, P. E., Moore, I. D., Mckenzie, N. J., and Ryan, P. J.: Soil-landscape modelling and spatial prediction of soil attributes, 9, 421–432, https://doi.org/10.1080/02693799508902047, 1995.

Gessler, P. E., Chadwick, O. A., Chamran, F., Althouse, L., and Holmes, K.: Modeling Soil-Landscape and Ecosystem Properties Using Terrain Attributes, 64, 2046–2056, https://doi.org/10.2136/sssaj2000.6462046x, 2000.

Gray, J. M., Bishop, T. F. A., and Smith, P. L.: Digital mapping of pre-European soil carbon stocks and decline since clearing over New South Wales, Australia, 54, 49–63, https://doi.org/10.1071/SR14307, 2016.

Guevara, M., Olmedo, G. F., Stell, E., Yigini, Y., Aguilar Duarte, Y., Arellano Hernández, C., Arévalo, G. E., Arroyo-Cruz, C. E., Bolivar, A., Bunning, S., Bustamante Cañas, N., Cruz-Gaistardo, C. O., Davila, F., Dell Acqua, M., Encina, A., Figueredo Tacona, H., Fontes, F., Hernández Herrera, J. A., Ibelles Navarro, A. R., Loayza, V., Manueles, A. M., Mendoza Jara, F., Olivera, C., Osorio Hermosilla, R., Pereira, G., Prieto, P., Ramos, I. A., Rey Brina, J. C., Rivera, R., Rodríguez-Rodríguez, J., Roopnarine, R., Rosales Ibarra, A., Rosales Riveiro, K. A., Schulz, G. A., Spence, A., Vasques, G. M., Vargas, R. R. R. R. R., Vargas, R. R. R. R. R., Federico Olmedo, G., Stell, E., Yigini, Y., Aguilar Duarte, Y., Arellano Hernández, C., Arévalo, G. E., Eduardo Arroyo-Cruz, C., Bolivar, A., Bunning, S., Bustamante Cañas, N., Omar Cruz-Gaistardo, C., Davila, F., Dell Acqua, M., Encina, A., Tacona, H. F., Fontes, F., Herrera, J. A. H., Roberto Ibelles Navarro, A., Loayza, V., Manueles, A. M., Mendoza Jara, F., Olivera, C., Osorio Hermosilla, R., Pereira, G., Prieto, P., Ramos, I. A., Carlos Rey Brina, J., Rivera, R., Rodríguez-

Rodríguez, J., Roopnarine, R., Ibarra, A. R., Amaury Rosales Riveiro, K., Andrés Schulz, G., Spence, A., Vasques, G. M., Vargas, R. R. R. R. R., and Vargas, R. R. R. R. R.: No silver bullet for digital soil mapping: Country-specific soil organic carbon estimates across Latin America, 4, 173–193, https://doi.org/10.5194/soil-4-173-2018, 2018.

Guyon, I., Weston, J., Barnhill, S., and Vapnik, V.: Gene selection for cancer classification using support vector machines, 46, 389–422, https://doi.org/10.1023/A:1012487302797, 2002.

Hartemink, A. E., Lowery, B., and Wacker, C.: Soil maps of Wisconsin, 189–190, 451–461, https://doi.org/10.1016/j.geoderma.2012.05.025, 2012.

Hawkins, D. M.: The problem of overfitting, 44, 1–12, https://doi.org/10.1021/ci0342472, 2004.

Hitziger, M. and Ließ, M.: Comparison of three supervised learning methods for digital soil mapping: Application to a complex terrain in the Ecuadorian Andes, 2014, 1–12, https://doi.org/10.1155/2014/809495, 2014.

Hugo, A., Barros, C., and Lier, Q. D. J. Van: Pedotransfer Functions for Brazilian Soils, in: Application of Soil Physics in Environmental Analyses, edited by: Teixeira, W. G., Ceddia, M. B., Ottoni, M. V., and Donnagema, G. K., Springer International Publishing, Cham, 131–162, https://doi.org/10.1007/978-3-319-06013-2, 2014.

Kempen, B., Brus, D.J., Stoorvogel, J.J., Heuvelink, G.B.M., de Vries, F., 2012. Efficiency comparison of conventional and digital soil mapping for updating soil maps. Soil Sci. Soc. Am. J. 76, 2097–2115.

Krinner, G., Viovy, N., de Noblet-Ducoudré, N., Ogée, J., Polcher, J., Friedlingstein, P., Ciais, P., Sitch, S., and Prentice, I. C.: A dynamic global vegetation model for studies of the coupled atmosphere-biosphere system, 19, https://doi.org/10.1029/2003GB002199, 2005.

Krysanova, V., Müller-Wohlfeil, D.-I., and Becker, A.: Development and test of a spatially distributed hydrological/water quality model for mesoscale watersheds, 106, 261–289, https://doi.org/10.1016/S0304-3800(97)00204-4, 1998.

Laurent, F., Poccard-Chapuis, R., Plassin, S., and Martinez, G. P.: Soil texture derived from topography in North-eastern Amazonia, 13, 109–115, https://doi.org/10.1080/17445647.2016.1266524, 2017.

Lagacherie, P., McBratney, A.B., 2006. Chapter 1 spatial soil information systems and spatial soil inference systems: Perspectives for digital soil mapping, in: Developments in Soil Science. Elsevier, pp. 3–22.

Li, J. and Heap, A. D.: Spatial interpolation methods applied in the environmental sciences: A review, 53, 173–189, https://doi.org/10.1016/j.envsoft.2013.12.008, 2014.

McBratney, A.B., Mendonça Santos, M.L., Minasny, B., 2003. On digital soil mapping. Geoderma 117, 3–52.

Tarboton, D.G., Bras, R.L., Rodriguez-Iturbe, I., 1991. On the extraction of channel networks from digital elevation data. Hydrol. Process. 5, 81–100.

McBratney, A. B., Mendonça Santos, M. L., and Minasny, B.: On digital soil mapping, 117, 3–52, https://doi.org/10.1016/S0016-7061(03)00223-4, 2003.

Mendonça-Santos, M. L. and Santos, H. G.: The State of the Art of Brazilian Soil Mapping and Prospects for Digital Soil Mapping, in: Developments in Soil Science, edited by: Lagacherie, P., McBratney, A. B., and Voltz, M., Elsevier, New York, USA, 39–55, https://doi.org/10.1016/S0166-2481(06)31003-3, 2006.

Montzka, C., Herbst, M., Weihermüller, L., Verhoef, A., and Vereecken, H.: A global data set of soil hydraulic properties and sub-grid variability of soil water retention and hydraulic conductivity curves, 9, 529–543, https://doi.org/10.5194/essd-9-529-2017, 2017.

Moore, I. D., Gessler, P. E., Nielsen, G. A., and Peterson, G. A.: Soil Attribute Prediction Using Terrain Analysis, 57, 443–452, https://doi.org/10.2136/sssaj1993.03615995005700020026x, 1993.

Natekin, A. and Knoll, A.: Gradient boosting machines, a tutorial, 7, 1–21, https://doi.org/10.3389/fnbot.2013.00021, 2013.

Nettesheim, F. C., Conto, T. de, Pereira, M. G., and Machado, D. L.: Contribution of Topography and Incident Solar Radiation to Variation of Soil and Plant Litter at an Area with Heterogeneous Terrain, 39, 750–762, https://doi.org/10.1590/01000683rbcs20140459, 2015.

Newman, A. C. D.: The significance of clays in agriculture and soils, 311, 375–389, https://doi.org/10.1098/rsta.1984.0035, 1984.

Oliveira, D. P., Sartor, L. R., Souza Júnior, V. S., Corrêa, M. M., Romero, R. E., Andrade, G. R. P., and Ferreira, T. O.: Weathering and clay formation in semi-arid calcareous soils from Northeastern Brazil, 162, 325–332, https://doi.org/10.1016/j.catena.2017.10.030, 2018.

Oliveira, L. B., Ribeiro, M. R., Jacomine, P. K. T., Rodrigues, J. J. V., and Marques, F. A.: Funções de pedotransferência para predição da umidade retida a potenciais específicos em solos do estado de Pernambuco, 26, 315–323, https://doi.org/10.1590/S0100-06832002000200004, 2002.

Oliveira, P., Machado, D. A., Cristina, E., and Fidalgo, C.: Estimativa da Densidade dos Solos Brasileiros, 2006.

Ottoni, M. V., Ottoni Filho, T. B., Schaap, M. G., Lopes-Assad, M. L. R. C., and Rotunno Filho, O. C.: Hydrophysical Database for Brazilian Soils (HYBRAS) and Pedotransfer Functions for Water Retention, 17, 170095, https://doi.org/10.2136/vzj2017.05.0095, 2018.

Overmars, K. P., de Groot, W. T., and Huigen, M. G. A.: Comparing Inductive and Deductive Modeling of Land Use Decisions: Principles, a Model and an Illustration from the Philippines, 35, 439–452, https://doi.org/10.1007/s10745-006-9101-6, 2007.

Padarian, J., Minasny, B., and McBratney, A. B.: Chile and the Chilean soil grid: A contribution to GlobalSoilMap, 9, 17–28, https://doi.org/10.1016/j.geodrs.2016.12.001, 2017.

Pahlavan-Rad, M. R., Dahmardeh, K., Hadizadeh, M., Keykha, G., Mohammadnia, N., Gangali, M., Keikha, M., Davatgar, N., and Brungard, C.: Prediction of soil water infiltration using multiple linear regression and random forest in a dry flood plain, eastern Iran, 194, 104715, https://doi.org/10.1016/j.catena.2020.104715, 2020.

Patton, N. R., Lohse, K. A., Godsey, S. E., Crosby, B. T., and Seyfried, M. S.: Predicting soil thickness on soil mantled hillslopes, 9, 3329, https://doi.org/10.1038/s41467-018-05743-y, 2018.

Poggio, L. and Gimona, A.: Assimilation of optical and radar remote sensing data in 3D mapping of soil properties over large areas, 579, 1094–1110, https://doi.org/10.1016/j.scitotenv.2016.11.078, 2017.

Poppiel, R. R., Demattê, J. A. M., Rosin, N. A., Campos, L. R., Tayebi, M., Bonfatti, B. R., Ayoubi, S., Tajik, S., Afshar, F. A., Jafari, A., Hamzehpour, N., Taghizadeh-Mehrjardi, R., Ostovari, Y., Asgari, N., Naimi, S., Nabiollahi, K., Fathizad, H., Zeraatpisheh, M., Javaheri, F., Doustaky, M., Naderi, M., Dehghani, S., Atash, S., Farshadirad, A., Mirzaee, S., Shahriari, A., Ghorbani, M., and Rahmati, M.: High resolution middle eastern soil attributes mapping via open data and cloud computing, 385, 114890, https://doi.org/10.1016/j.geoderma.2020.114890, 2021.

Pribyl, D. W.: A critical review of the conventional SOC to SOM conversion factor, 156, 75–83, https://doi.org/10.1016/j.geoderma.2010.02.003, 2010.

Rahmati, M., Weihermüller, L., Vanderborght, J., Pachepsky, Y. A., Mao, L., Sadeghi, S. H., Moosavi, N., Kheirfam, H., Montzka, C., Van Looy, K., Toth, B., Hazbavi, Z., Al Yamani, W., Albalasmeh, A. A., Alghzawi, M. Z., Angulo-Jaramillo, R., Antonino, A. C. D., Arampatzis, G., Armindo, R. A., Asadi, H., Bamutaze, Y., Batlle-Aguilar, J., Béchet, B., Becker, F., Blöschl, G., Bohne, K., Braud, I., Castellano, C., Cerdà, A., Chalhoub, M., Cichota, R., Císlerová, M., Clothier, B., Coquet, Y., Cornelis, W., Corradini, C., Coutinho, A. P., de Oliveira, M. B., de Macedo, J. R., Durães, M. F., Emami, H., Eskandari, I., Farajnia, A., Flammini, A., Fodor, N., Gharaibeh, M., Ghavimipanah, M. H., Ghezzehei, T. A., Giertz, S., Hatzigiannakis, E. G., Horn, R., Jiménez, J. J., Jacques, D., Keesstra, S. D., Kelishadi, H., Kiani-Harchegani, M., Kouselou, M., Kumar Jha, M., Lassabatere, L., Li, X., Liebig, M. A., Lichner, L., López, M. V., Machiwal, D., Mallants, D., Mallmann, M. S., de Oliveira Marques, J. D., Marshall, M. R., Mertens, J., Meunier, F., Mohammadi, M. H., Mohanty, B. P., Pulido-Moncada, M., Montenegro, S., Morbidelli, R., Moret-Fernández, D., Moosavi, A. A., Mosaddeghi, M. R., Mousavi, S. B., Mozaffari, H., Nabiollahi, K., Neyshabouri, M. R., Ottoni, M. V., Ottoni Filho, T. B., Pahlavan-Rad, M. R., Panagopoulos, A., Peth, S., Peyneau, P.-E., Picciafuoco, T., Poesen, J., Pulido, M., Reinert, D. J., Reinsch, S., Rezaei, M., Roberts, F. P., Robinson, D., Rodrigo-Comino, J., Rotunno Filho, O. C., Saito, T., et al.: Development and analysis of the Soil Water Infiltration Global database, 10, 1237–1263, https://doi.org/10.5194/essd-10-1237-2018, 2018.

Ramifehiarivo, N., Brossard, M., Grinand, C., Andriamananjara, A., Razafimbelo, T., Rasolohery, A., Razafimahatratra, H., Seyler, F., Ranaivoson, N., Rabenarivo, M., Albrecht, A., Razafindrabe, F., and Razakamanarivo, H.: Mapping soil organic carbon on a national scale: Towards an improved and updated map of Madagascar, 9, 29–38, https://doi.org/10.1016/j.geodrs.2016.12.002, 2017.

Ravi, S., D'Odorico, P., Over, T. M., and Zobeck, T. M.: On the effect of air humidity on soil susceptibility to wind erosion: The case of air-dry soils, 31, n/a-n/a, https://doi.org/10.1029/2004GL019485, 2004.

Richards, J. A.: Remote Sensing Digital Image Analysis, 5th ed., Springer Berlin Heidelberg, Berlin, Heidelberg, 494 pp., https://doi.org/10.1007/978-3-642-30062-2, 2013.

Salgueiro, J. H. P. de B., Montenegro, S. M. G. L., Pinto, E. J. de A., Silva, B. B. da, Souza, W. M. de, and Oliveira, L. M. M. de: Influence of oceanic-atmospheric interactions on extreme events of daily rainfall in the Sub-basin 39 located in Northeastern Brazil, 21, 685–693, https://doi.org/10.1590/2318-0331.011616023, 2016.

Saxton, K. E. and Rawls, W. J.: Soil Water Characteristic Estimates by Texture and Organic Matter for Hydrologic Solutions, 70, 1569, https://doi.org/10.2136/sssaj2005.0117, 2006.

Scull, P., Franklin, J., Chadwick, O. A., and McArthur, D.: Predictive soil mapping: A review, 27, 171–197, https://doi.org/10.1191/0309133303pp366ra, 2003.

Sharpley, A. N. and Williams, J. R.: EPIC-Erosion/Productivity Impact Calculator: 1. Model Documentation, in: U.S. Department of Agriculture Technical Bulletin, 235, 1990.

Silva, F. B. R., Santos, J. C. P., Silva, A. B., Calvacanti, A. C., Silva, F. H. B. B., Burgos, N., Parahyba, R. B. V., Oliveira Neto, M. B., Souza Neto, N. C., Araújo Filho, J. C., Lopes, O. F., Luz, L. R. Q. P., Leite, A. P., Souza, L. G. M. C., Silva, C. P., Varejão-Silva, M. A., and Barros, A. H. C.: Zoneamento agroecológico do Estado de Pernambuco, 2001.

Souza, A. G. S. S., Ribeiro Neto, A., and Souza, L. L. de: Soil moisture-based index for agricultural drought assessment: SMADI application in Pernambuco State-Brazil, 252, 112124, https://doi.org/10.1016/j.rse.2020.112124, 2021.

Project MapBiomas - Collection 5 of Brazilian Land Cover & Use Map Series: https://mapbiomas.org/en.

Souza, C. M., Z. Shimbo, J., Rosa, M. R., Parente, L. L., A. Alencar, A., Rudorff, B. F. T., Hasenack, H., Matsumoto, M., G. Ferreira, L., Souza-Filho, P. W. M., de Oliveira, S. W., Rocha, W. F., Fonseca, A. V., Marques, C. B., Diniz, C. G., Costa, D., Monteiro, D., Rosa, E. R., Vélez-Martin, E., Weber, E. J., Lenti, F. E. B., Paternost, F. F., Pareyn, F. G. C., Siqueira, J. V., Viera, J. L., Neto, L. C. F., Saraiva, M. M., Sales, M. H., Salgado, M. P. G., Vasconcelos, R., Galano, S., Mesquita, V. V., and Azevedo, T.: Reconstructing Three Decades of Land Use and Land Cover Changes in Brazilian Biomes with Landsat Archive and Earth Engine, 12, 2735, https://doi.org/10.3390/rs12172735, 2020.

Souza, R., Feng, X., Antonino, A., Montenegro, S., Souza, E., and Porporato, A.: Vegetation response to rainfall seasonality and interannual variability in tropical dry forests, 30, 3583–3595, https://doi.org/10.1002/hyp.10953, 2016.

Tarboton, D.G., Bras, R.L., Rodriguez-Iturbe, I., 1991. On the extraction of channel networks from digital elevation data. Hydrol. Process. 5, 81–100.

Taghizadeh-mehrjardi, R., Nabiollahi, K., and Kerry, R.: Geoderma Digital mapping of soil organic carbon at multiple depths using different data mining techniques in Baneh region, Iran, 266, 98–110, https://doi.org/10.1016/j.geoderma.2015.12.003, 2016.

Tan, J., Xie, X., Zuo, J., Xing, X., Liu, B., Xia, Q., and Zhang, Y.: Coupling random forest and inverse distance weighting to generate climate surfaces of precipitation and temperature with Multiple-Covariates, 598, 126270, https://doi.org/10.1016/j.jhydrol.2021.126270, 2021.

Teng, H. T., Viscarra Rossel, R. A., Shi, Z., and Behrens, T.: Updating a national soil classification with spectroscopic predictions and digital soil mapping, 164, 125–134, https://doi.org/10.1016/j.catena.2018.01.015, 2018.

Tomasella, J. and Hodnett, M. G.: Estimating soil water retention characteristics from limited data in Brazilian Amazonia, 163, 1998.

Tomasella, J., Hodnett, M. G., and Rossato, L.: Pedotransfer Functions for the Estimation of Soil Water Retention in Brazilian Soils, 64, 327, https://doi.org/10.2136/sssaj2000.641327x, 2000.

Torres, F. S. de M.: Geodiversidade do estado de Pernambuco, 1st ed., edited by: Torres, F. S. de M. and Pfaltzgraff, P. A. dos S., CPRM, Recife, 282 pp., 2014.

Tóth, B., Weynants, M., Pásztor, L., and Hengl, T.: 3D soil hydraulic database of Europe at 250 m resolution, 31, 2662–2666, https://doi.org/10.1002/hyp.11203, 2017.

Truu, M., Ostonen, I., Preem, J.-K., Lõhmus, K., Nõlvak, H., Ligi, T., Rosenvald, K., Parts, K., Kupper, P., and Truu, J.: Elevated Air Humidity Changes Soil Bacterial Community Structure in the Silver Birch Stand, 8, https://doi.org/10.3389/fmicb.2017.00557, 2017.

Valeriano, M. M. de and Rossetti, D. F. de: Topodata: Brazilian full coverage refinement of SRTM data, 32, 300–309, https://doi.org/10.1016/j.apgeog.2011.05.004, 2012.

van Genuchten, M.T., 1980. A Closed-form Equation for Predicting the Hydraulic Conductivity of Unsaturated Soils. Soil Science Society of America Journal 44, 892–898.

Vieira, S. R.: Geoestatística em estudos de variabilidade espacial do solo, in: Tópicos em ciência do solo, edited by: Novais, R. F., Alvarez, V. H., and Schaefer, C. E. G. R., Sociedade Brasileira de Ciência do Solo, Viçosa, 1–54, 2000.

De Vos, B., Van Meirvenne, M., Quataert, P., Deckers, J., and Muys, B.: Predictive Quality of Pedotransfer Functions for Estimating Bulk Density of Forest Soils, 69, 500–510, https://doi.org/10.2136/sssaj2005.0500, 2005.

Wang, Q., Wu, B., Stein, A., Zhu, L., and Zeng, Y.: Soil depth spatial prediction by fuzzy soil-landscape model, 18, 1041–1051, https://doi.org/10.1007/s11368-017-1779-0, 2018.

Wang, Y. P., Kowalczyk, E., Leuning, R., Abramowitz, G., Raupach, M. R., Pak, B., van Gorsel, E., and Luhar, A.: Diagnosing errors in a land surface model (CABLE) in the time and frequency domains, 116, G01034, https://doi.org/10.1029/2010JG001385, 2011.

Whitney, A. W.: A Direct Method of Nonparametric Measurement Selection, C–20, 1100–1103, https://doi.org/10.1109/T-C.1971.223410, 1971.

Wong, T.-T.: Performance evaluation of classification algorithms by k-fold and leave-one-out cross validation, 48, 2839–2846, https://doi.org/10.1016/j.patcog.2015.03.009, 2015.

Yost, J. L. and Hartemink, A. E.: How deep is the soil studied – an analysis of four soil science journals, 452, 5–18, https://doi.org/10.1007/s11104-020-04550-z, 2020.

Zeraatpisheh, M., Ayoubi, S., Jafari, A., Tajik, S., and Finke, P.: Digital mapping of soil properties using multiple machine learning in a semi-arid region, central Iran, 338, 445–452, https://doi.org/10.1016/j.geoderma.2018.09.006, 2019.

Ziadat, F. M.: Prediction of Soil Depth from Digital Terrain Data by Integrating Statistical and Visual Approaches, 20, 361–367, https://doi.org/10.1016/S1002-0160(10)60025-2, 2010.

Ziadat, F. M., Dhanesh, Y., Shoemate, D., Srinivasan, R., Narasimhan, B., and Tech, J.: Soil-landscape estimation and evaluation program (SLEEP) to predict spatial distribution of soil attributes for environmental modeling, 8, 1–15, https://doi.org/10.3965/j.ijabe.20150803.1270, 2015.

Zobeck, T., Fryrear, D., and Pettit, R. D.: Management effects on wind-eroded sediment and plant nutrients, 44, 160–163, 1989.